

## A Universal Model for Spike-Frequency Adaptation

**Jan Benda**

*j.benda@biologie.hu-berlin.de*

*Department of Physics, University of Ottawa, Ottawa, Ontario, K1N 6N5, Canada*

**Andreas V. M. Herz**

*a.herz@biologie.hu-berlin.de*

*Institute for Theoretical Biology, Humboldt University Berlin, 10115 Berlin, Germany*

**Spike-frequency adaptation is a prominent feature of neural dynamics. Among other mechanisms, various ionic currents modulating spike generation cause this type of neural adaptation. Prominent examples are voltage-gated potassium currents (M-type currents), the interplay of calcium currents and intracellular calcium dynamics with calcium-gated potassium channels (AHP-type currents), and the slow recovery from inactivation of the fast sodium current. While recent modeling studies have focused on the effects of specific adaptation currents, we derive a universal model for the firing-frequency dynamics of an adapting neuron that is independent of the specific adaptation process and spike generator. The model is completely defined by the neuron's onset  $f$ - $I$  curve, the steady-state  $f$ - $I$  curve, and the time constant of adaptation. For a specific neuron, these parameters can be easily determined from electrophysiological measurements without any pharmacological manipulations. At the same time, the simplicity of the model allows one to analyze mathematically how adaptation influences signal processing on the single-neuron level. In particular, we elucidate the specific nature of high-pass filter properties caused by spike-frequency adaptation. The model is limited to firing frequencies higher than the reciprocal adaptation time constant and to moderate fluctuations of the adaptation and the input current. As an extension of the model, we introduce a framework for combining an arbitrary spike generator with a generalized adaptation current.**

### 1 Introduction ---

Spike-frequency adaptation is a widespread neurobiological phenomenon, exhibited by almost any type of neuron that generates action potentials. It occurs in vertebrates as well as in invertebrates, in peripheral as well as in central neurons, and it may play an important role in neural information processing. Within the large variety of mechanisms responsible for spike-frequency adaptation, ionic currents that influence spike generation

are of particular importance. Three main types of such adaptation currents are known: M-type currents, which are caused by voltage-dependent, high-threshold potassium channels (Brown & Adams, 1980); AHP-type currents, mediated by calcium-dependent potassium channels (Madison & Nicoll, 1984); and slow recovery from inactivation of the fast sodium channel (Fleiderer, Friedman, & Gutnick, 1996).

Recent computer simulations and analytical studies have focused on specific adaptation mechanisms (Cartling, 1996; Wang, 1998; Ermentrout, 1998; Ermentrout, Pascal, & Gutkin, 2001). To complement these approaches, we investigate a large group of potential cellular mechanisms. Our goal is to derive a single universal model that is independent of the biophysical processes underlying adaptation.

Such a framework has various advantages from both an experimental and a theoretical point of view. For example, it is often desirable to quantify spike-frequency adaptation without performing pharmacological manipulations to characterize specific adaptation currents (Benda, Bethge, Hennig, Pawelzik, & Herz, 2001). This is particularly true if these currents have not yet been identified in detail. Furthermore, a low-dimensional phenomenological model is well suited for systematic network simulations and may thus help to elucidate the functional role of cellular adaptation on the systems level.

The phenomenon of spike-frequency adaptation is illustrated in Figure 1. Let us assume that the investigated neuron is in a fully unadapted state. The initial response to a step-like stimulus reflects the properties of the nonadapted cell, which are determined by the fast processes of the spike generator only. The resulting behavior is covered by the neuron's onset  $f$ - $I$  curve  $f_0(I)$ , which describes the initial firing frequency  $f_0$  as a function of the stimulus intensity  $I$ . Due to adaptation, the firing frequency  $f$  decays to some steady-state value  $f_\infty$ . The neuron may even stop spiking after a while. Measuring  $f_\infty$  for different inputs  $I$  results in the steady-state  $f$ - $I$  curve  $f_\infty(I)$ . Electrophysiological recordings show that the decay of the firing frequency is often approximately exponential and characterized by some effective adaptation time constant  $\tau_{\text{eff}}$ , which may range from tens of milliseconds (Madison & Nicoll, 1984; Stocker, Krause, & Pedarzini, 1999) to several seconds (Edman, Gastrelus, & Grampp, 1987; Sah & Clements, 1999). The model we are going to derive is completely defined by the onset  $f$ - $I$  curve  $f_0(I)$ , the steady-state  $f$ - $I$  curve  $f_\infty(I)$ , and the effective time constant  $\tau_{\text{eff}}$ . These quantities can be easily measured experimentally and thus allow quickly characterizing the adaptation properties of individual neurons.

The article is organized as follows. In section 2, we extract generic properties of three prototypical adaptation mechanisms. This allows us to derive a universal phenomenological model in section 3. In section 4, we investigate how the parameters of the model are related to the neuron's  $f$ - $I$  curves and how the adaptation time constant can be estimated experimentally.

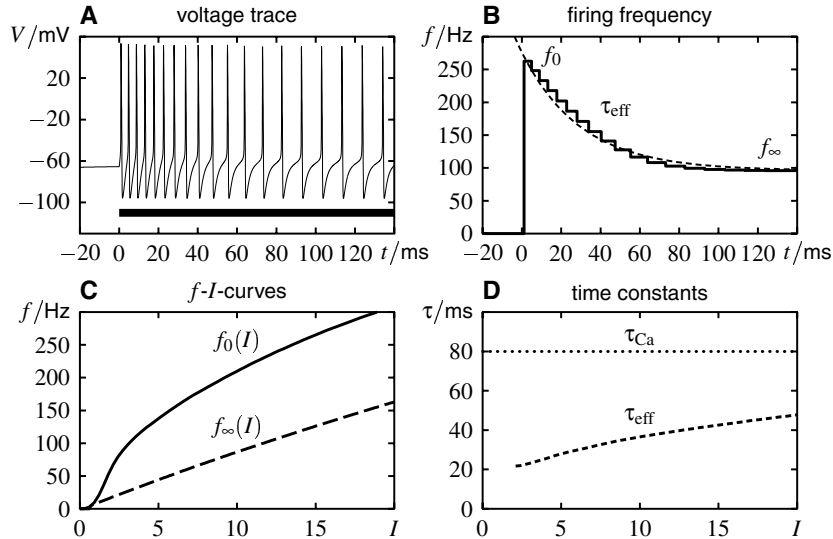


Figure 1: The phenomenon of spike-frequency adaptation. (A) The voltage trace of a modified Traub-Miles model with mAHP current (see the appendix for details) evoked by a step-like stimulus ( $I = 18 \mu\text{A}/\text{cm}^2$ ) as indicated by the solid bar. (B) The corresponding instantaneous firing frequency, defined as the reciprocal of the interspike intervals. The response  $f$  decays from its onset value  $f_0$  in an approximately exponential manner (dashed line) with an effective time constant  $\tau_{\text{eff}}$  to a steady-state value  $f_\infty$ . (C) Measuring the onset and steady-state response at different stimulus intensities results in the onset and the steady-state  $f$ - $I$  curves,  $f_0(I)$  and  $f_\infty(I)$ , respectively. (D)  $\tau_{\text{eff}}$  depends on input intensity  $I$  and is much smaller than the time constant  $\tau_{\text{Ca}}$  of the calcium removal, which determines the dynamics of adaptation in the model used for this simulation.

Based on the model, we analyze the effect of adaptation on the neuron's  $f$ - $I$  curves and quantify signal transmission properties arising from adaptation in section 5. Section 6 extends our results and shows how the adaptation model can be combined with models of spike generation. We discuss the model in section 7. A list of commonly used symbols is given in the appendix.

To illustrate our results we use a modified Traub-Miles model (Ermentrout, 1998) as well as the Crook model (Crook, Ermentrout, & Bower, 1998). We add either an M-type current or an mAHP current to simulate spike-frequency adaptation. The dynamical equations and parameter values are also summarized in the appendix.

## 2 General Characteristics of Adaptation Currents

---

In this section, we examine three basic types of ionic currents causing spike-frequency adaptation: M-type currents, mAHP-type currents, and sodium currents with slow recovery from inhibition. Our goal is to show that these different mechanisms can be described by an effective adaptation current  $I_A$ :

$$I_A = \bar{g}_A m^p h^q c a (V - E_A) \quad (2.1a)$$

$$\tau_a(V) \frac{da}{dt} = a_\infty(V) - a. \quad (2.1b)$$

As in the following, the time dependence of dynamical variables has been omitted for simplicity.  $\bar{g}_A$  is the current's maximum conductance and  $E_A$  is its reversal potential. The dynamics (2.1b) of the adaptation gating variable  $a$  is a simple relaxation toward a voltage-dependent steady-state variable  $a_\infty(V)$  with a time constant  $\tau_a(V)$  that could depend on the membrane potential  $V$ .  $m$  and  $h$  are possible additional voltage gated variables raised to the integer power  $p$  and  $q$ , respectively. Both variables, if present, have to be much faster than the adaptation variable  $a$ . The constant  $c$  is a proportionality factor for  $a$ . In essence, equations (2.1) are the well-known equations for a voltage gated current as introduced by Hodgkin and Huxley (1952).

**2.1 M-Type Currents.** M-type currents are slow voltage-dependent potassium currents (Brown & Adams, 1980). Their dynamics is captured by

$$I_M = \bar{g}_M a (V - E_M) \quad (2.2a)$$

$$\tau_a(V) \frac{da}{dt} = a_\infty(V) - a, \quad (2.2b)$$

where  $\bar{g}_M$  denotes the maximum conductance and  $E_M$  the reversal potential. The steady-state variable  $a_\infty(V)$  is a sigmoidal function of the membrane potential  $V$  with values between zero and one. M-type currents are mainly activated during a spike (see Figures 2 and 3). Between spikes, they deactivate slowly as determined by their time constant  $\tau_a(V)$ . Activation of M-type currents causes spike-frequency adaptation, since as potassium currents they decrease the sensitivity of the spike generator to input currents. Equations (2.2) are a simple realization of the general description (2.1), with  $a$  being the only gating variable and  $c = 1$ .

**2.2 mAHP Currents.** An important adaptation mechanism arises from medium afterhyperpolarization (mAHP) currents, which are calcium-dependent potassium currents (Madison & Nicoll, 1984). Three processes are involved in this type of adaptation.

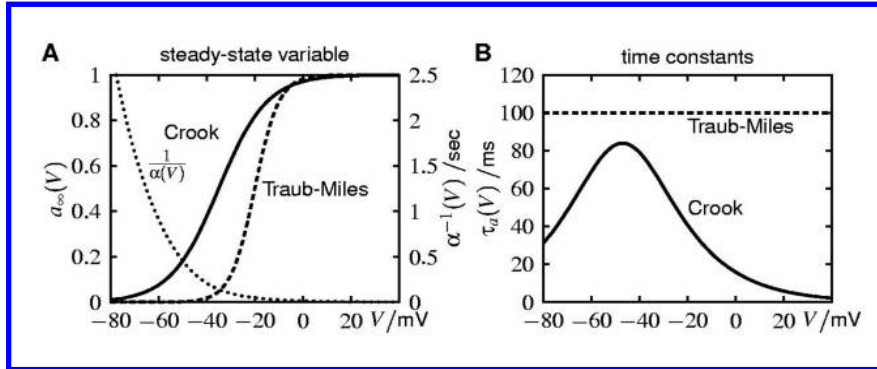


Figure 2: Properties of M-type currents. (A) The dependence of the activation function  $a_\infty(V)$  on the membrane potential  $V$  as defined in the Crook model and the modified Traub-Miles model. While in the Crook model the M-type current is slightly activated even at rest ( $V_{\text{rest}} = -71.4$  mV), in the modified Traub-Miles model, it is activated only during spikes ( $V_{\text{rest}} = -66.5$  mV). The dotted line is the inverse rate constant  $\alpha(V)$  of the M-type current in the Crook model, given in seconds. (B) The time constant  $\tau_a(V)$  in the Crook model is the product of  $a_\infty(V)$  and  $1/\alpha(V)$  shown in A and has a peak within the linear range of  $a_\infty(V)$ . In the modified Traub-Miles model,  $\tau_a(V)$  is assumed to be constant.

First, there are different voltage-gated calcium channels (N, P, Q, L and T type) that are rapidly activated by depolarizations (about 1 millisecond; Jaffe et al., 1994). Recent calcium imaging studies show that the total calcium influx per spike is approximately constant (Schiller, Helmchen, & Sakmann, 1995; Helmchen, Imoto, & Sakmann, 1996). Calcium-induced calcium release may also contribute to spike-triggered calcium transients (Sandler & Barbara, 1999). All of these processes are very fast. They can be viewed as part of the spike generator and do not lead to adaptation. In the context of adaptation, the only relevant effect of these currents is that they increase the intracellular calcium concentration.

Second, calcium is removed with a slow time constant  $\tau_{\text{Ca}}$ . This process is the result of buffering, diffusion, and calcium pumps and can be described by

$$\tau_{\text{Ca}} \frac{d[\text{Ca}^{2+}]}{dt} = \beta I_{\text{Ca}} - [\text{Ca}^{2+}]; \quad (2.3)$$

that is, the concentration of intracellular calcium  $[\text{Ca}^{2+}]$  is increased proportionally to the calcium influx  $I_{\text{Ca}}$  (Traub, Wong, Miles, & Michelson, 1991). The time constant  $\tau_{\text{Ca}}$  of the calcium removal determines the timescale of this type of adaptation. Thus, the calcium dynamics 2.3 is equivalent to the dynamics 2.2b of the gating variable  $a$  of an M-type current.

Finally, a potassium current  $I_{\text{AHP}}$  is activated depending on the intracellular calcium concentration (Brown & Griffith, 1983; Madison & Nicoll,

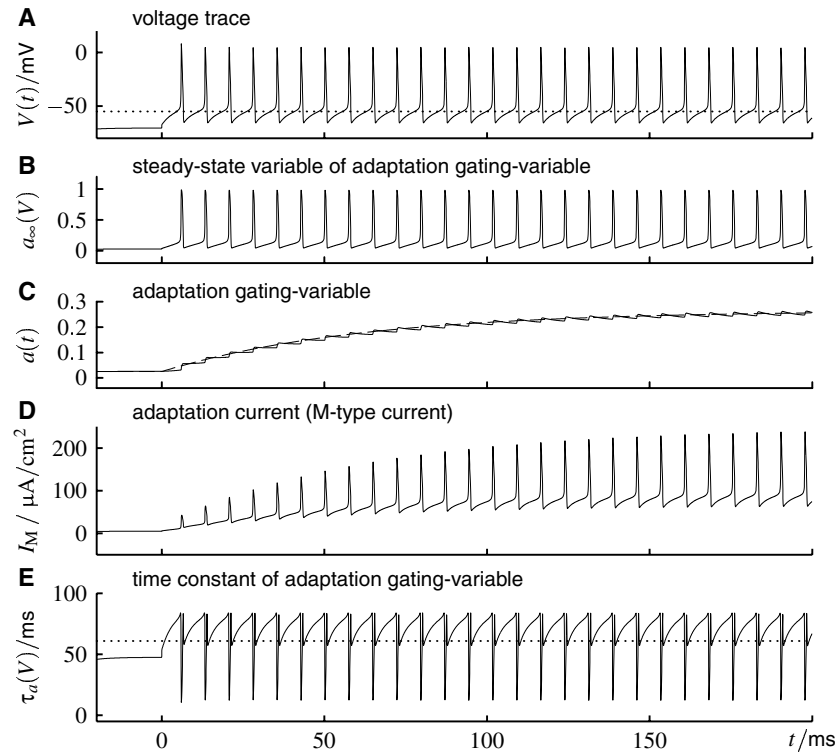


Figure 3: The dynamics of an adaptation current. Shown is a simulation of the Crook model stimulated with a constant current  $I = 4 \mu\text{A}/\text{cm}^2$  starting at  $t = 0$ . Only the sodium, potassium, and calcium currents are included in the membrane equation so that the firing frequency is constant and does not adapt. To illustrate the generic behavior of adaptation currents, *B–E* display the dynamical variables of an M-type current activated by the voltage trace shown in *A*. The steady-state variable  $a_\infty(V)$  and the time constant  $\tau_a(V)$  used to model the M-type current are shown in Figure 2. (A) Voltage trace. The dotted straight line marks the potential above which  $a_\infty(V)$  is activated. (B) The time course of  $a_\infty(V)$  resulting from the voltage trace in *A*. (C) Due to the fast deflections of  $a_\infty(V)$ , the adaptation gating-variable  $a$  increases rapidly during spikes. Between the spikes,  $a$  decays with the time constant  $\tau_a(V)$  shown in *E*. The time course of  $a$  can be well approximated by its running average  $\langle a \rangle_T$ , which is roughly exponential (dashed line) with a time constant of 61 ms in this simulation. (D) The adaptation current  $I_M = \bar{g}_M a (V - E_M)$ . Note its large fluctuations caused by the spike activity. (E) The time constant  $\tau_a(V)$  also fluctuates strongly during the spikes. The dotted line denotes the value of the time constant corresponding to the mean gating variable in *C*.

1984):

$$I_{\text{AHP}} = \bar{g}_{\text{AHP}} q(V - E_{\text{K}}) \quad (2.4a)$$

$$\tau_q([\text{Ca}^{2+}]) \frac{dq}{dt} = q_{\infty}([\text{Ca}^{2+}]) - q \quad (2.4b)$$

This mAHP current is responsible for spike-frequency adaptation. Due to the slow calcium dynamics 2.3,  $q_{\infty}([\text{Ca}^{2+}])$  is also changing slowly. The time constant  $\tau_q$ , however, is much smaller than the time constant  $\tau_{\text{Ca}}$  of the calcium removal. Thus, we can approximate the gating variable  $q$  by its steady-state variable  $q_{\infty}([\text{Ca}^{2+}])$ . As the analysis of various models shows,  $q_{\infty}([\text{Ca}^{2+}])$  is well captured by a first-order Michaelis-Menten function and takes only small values (Crook et al., 1998; Ermentrout, 1998). Therefore, we can approximate it by  $q_{\infty}([\text{Ca}^{2+}]) \approx c \cdot [\text{Ca}^{2+}]$  where  $c > 0$ .

With these approximations, an mAHP-type current can be summarized as

$$I_{\text{AHP}} \approx \bar{g}_{\text{AHP}} c [\text{Ca}^{2+}] (V - E_{\text{K}}) \quad (2.5a)$$

$$\tau_{\text{Ca}} \frac{d[\text{Ca}^{2+}]}{dt} = \beta I_{\text{Ca}}(V) - [\text{Ca}^{2+}]. \quad (2.5b)$$

Since the calcium currents are fast, the calcium influx  $I_{\text{Ca}}$  has been approximated by a function directly depending on the membrane potential. The dynamics of mAHP-type currents are thus formally equal to those of an M-type current.

**2.3 Slow Recovery from Inactivation.** Slow recovery from inactivation of fast sodium channels is caused by an additional inactivation of the sodium current, which is much slower than the Hodgkin-Huxley-type inactivation  $h$ . It induces a use-dependent removal of excitable sodium channels and results in spike-frequency adaptation (Fleidervish et al., 1996).

Such currents are gated by an activation variable  $m$  and inactivation variable  $h$ , and an additional slow inactivation variable  $s$ :

$$I_{\text{Na}} = \bar{g}_{\text{Na}} m^3 h s (V - E_{\text{Na}}) \quad (2.6a)$$

$$\tau_m(V) \frac{dm}{dt} = m_{\infty}(V) - m \quad (2.6b)$$

$$\tau_h(V) \frac{dh}{dt} = h_{\infty}(V) - h \quad (2.6c)$$

$$\tau_s(V) \frac{ds}{dt} = s_{\infty}(V) - s. \quad (2.6d)$$

The time constant  $\tau_m$  of the activation variable  $m$  is shorter than 1 millisecond, and  $\tau_h$  is of the order of a few milliseconds (Hodgkin & Huxley, 1952;

Martina & Jonas, 1997). In contrast, the time constant  $\tau_s$  of the slow inactivation process  $s$  ranges from a few 100 ms (Martina & Jonas, 1997; Fleidervish et al., 1996) to more than 1 second (Edman et al., 1987; French, 1989).

Substituting the term  $(1 - a)$  for the slow inactivation gating variable  $s$  results in

$$I_{\text{Na}} = \bar{g}_{\text{Na}} m^3 h (V - E_{\text{Na}}) - \bar{g}_{\text{Na}} m^3 h a (V - E_{\text{Na}}) \quad (2.7a)$$

$$\tau_s(V) \frac{da}{dt} = 1 - s_{\infty}(V) - a. \quad (2.7b)$$

By this transformation, we have formally split  $I_{\text{Na}}$  into two components. The first one depends on only the two fast gating variables  $m$  and  $h$ , and is responsible for spike initiation only. The second component depends on the two fast gating variables  $m$  and  $h$  and on the gating variable  $a$ . The time constant  $\tau_s(V)$  of the dynamics (2.7b) of  $a$  is voltage dependent and much slower than the spike generator. The steady-state variable  $1 - s_{\infty}(V)$  is mainly activated at depolarized potentials, that is, during spikes. Thus, this second component causes adaptation. It conforms with the general adaptation current (2.1a) with  $c = -1$ . The dynamics (2.7b) resembles that of an M-type current (2.2b).

The adaptation current differs from the spike-initiating component in equation (2.7a) by the factor  $a$ . Under realistic conditions,  $a$  never gets close to its maximum value, which is unity, since very high sustained firing frequencies would be required to do so. Therefore, most of the time, the adaptation current is smaller than the spike-initiating component. Because  $V$  always stays below the reversal potential of the sodium current, the driving force  $V - E_{\text{Na}}$  is negative so that the second component in equation 2.7a is positive as the M-type current.

### 3 Universal Phenomenological Model

The previous section showed that three fundamental adaptation mechanisms can be reduced to a single current (2.1a), which is gated by a single variable obeying a first-order differential equation, (2.1b). We now go one step further and derive a phenomenological model for the firing frequency of an adapting neuron, whose parameters are independent of the specific adaptation process. To achieve this goal, we replace the adaptation gating variable  $a$  as well as the adaptation current  $I_A$  by suitable time averages. All the dependencies on the membrane potential can then be replaced by functions depending on the firing frequency  $f$ . The resulting universal model for spike-frequency adaptation reads

$$f = f_0(I - A \cdot [1 + \gamma(f)]) \quad (3.1a)$$

$$\tau \cdot [1 + \epsilon(f)] \frac{dA}{dt} = A_{\infty}(f) - A. \quad (3.1b)$$

The adaptation state  $A$  generalizes the averaged adaptation gating variable  $a$  and decays with an adaptation time constant  $\tau$  toward the steady-state adaptation strength  $A_\infty$ , which depends on the current firing frequency  $f$ . The averaged adaptation current  $A \cdot [1 + \gamma(f)]$  depends linearly on  $A$  and may be influenced by  $f$  through  $\gamma(f)$ . The term  $\epsilon(f)$  covers a potential dependence of  $\tau$  on  $f$ . The input current  $I$  minus the averaged adaptation current is mapped through the neuron's onset  $f$ - $I$  curve  $f_0(I)$  to result in the firing frequency  $f$ .

In the next section, we first motivate equation (3.1a). We then derive the simplified adaptation current and its dynamics (3.1b) from the general adaptation current, equations 2.1.

**3.1 Spike Generator and Firing Frequency.** Let us first consider a spiking neuron that does not adapt at all (see Figure 3A). The neuron contains only fast ion channels responsible for spike generation. The membrane potential  $V$  at the neuron's spike initiating zone evolves according to

$$C \frac{dV}{dt} = - \sum_i g_i (V - E_i) + I. \quad (3.2)$$

The parameter  $C$  is the membrane capacitance. Ionic currents of type  $i$  are characterized by a reversal potential  $E_i$  and a conductance  $g_i$ , whose dynamics is described by further differential equations (Hodgkin & Huxley, 1952; Johnston & Wu, 1997). The input current  $I$  can be viewed as a dendritic current, a synaptic current, or a current injected through a microelectrode.

In general, the membrane equation, 3.2, cannot be solved analytically. However, we do not need to know the exact time course of the membrane potential, because we are interested only in times at which spikes occur. For strong enough input, the neuron fires repetitively with firing frequency  $f$  (Hodgkin, 1948). For constant or slowly varying stimulus  $I(t)$ , this is captured by the neuron's  $f$ - $I$  curve,

$$f(t) = f_0(I(t)), \quad (3.3)$$

the simplest transformation of an input current into spikes. In the following, we use equation 3.3 to indicate that the spike generator transforms the input signal into a sequence of spikes from which a firing frequency  $f(t)$  can be computed. We discuss this process and the validity of equation 3.3 in more detail in section 6. The main advantage of using the neuron's  $f$ - $I$  curve to characterize its encoding properties is that for real neurons, the  $f$ - $I$  curve can be easily obtained from electrophysiological recordings.

Adding an adaptation current (2.1a) can be viewed as adding a second input current. Formally, the firing frequency of the neuron is then given by

$$f = f_0(I - I_A) = f_0(I - \bar{g}_A m^p h^q c a (V - E_A)). \quad (3.4)$$

This provides a first hint that the main effect of an adaptation current may be a shift of the neuron's  $f$ - $I$  curve in the direction of higher input currents  $I$ .

Equation (3.4) is, however, insufficient for a model that involves firing frequency only, since it still contains  $m$ ,  $h$ , and  $V$ . As a next step, we show how the adaptation current can be replaced by a suitable average that no longer depends on the spike generator.

**3.2 Averaging the Adaptation Current.** Since the overall evolution of the adaptation gating variable  $a$  is slow compared to spike generation (see, for example, Figure 3C), we may try to separate both subsystems and replace  $a$  by its running average  $\langle a \rangle_T$  over one period  $T$  of the fast subsystem

$$a(t) \approx \langle a \rangle_T(t) := \frac{1}{T(t)} \int_{t-T(t)/2}^{t+T(t)/2} a(t') dt', \quad (3.5)$$

where  $T(t)$  denotes the time-dependent interspike interval (ISI). To allow this distinction between a fast and a slow dynamics,  $T(t)$  has to be short compared to the time constant of the adaptation processes, which is true for sufficiently high firing frequencies. This key assumption implies that the spike generator is operating in its super-threshold regime.

We next aim at replacing the adaptation current  $I_A$  in equation 2.1a by a suitable average,

$$\langle I_A \rangle_{T,w} = \int_0^T w(t) I_A(t) dt, \quad (3.6)$$

where the normalized weight function  $w(t)$ ,  $\int_0^T w dt = 1$ , is chosen such that  $\langle I_A \rangle_{T,w}$  does not change the effect on the resulting firing frequency. Inserting the general adaptation current (2.1a) and replacing  $a$  by its time average 3.5 we obtain

$$\langle I_A \rangle_{T,w} = \langle \bar{g}_A m^p h^q c \langle a \rangle_T (V - E_A) \rangle_{T,w} \quad (3.7)$$

where we can move  $\bar{g}_A c \langle a \rangle_T$  out of the average. Then equation 3.7 represents an average over the variables  $V$ ,  $m$ , and  $h$  of the spike generator only.

If the effect of the adaptation current on the time course of these variables is approximately independent of the specific value of  $\langle a \rangle_T$ , then there exists a weight function that is independent of adaptation; the weight is solely a property of the spike generator. This is the second assumption needed for the separation of the fast spiking and the slow adaptation dynamics. It implies that the adaptation current simply reduces the input current and that fluctuations of the adaptation current have a negligible effect on the time course of the spike generator. This assumption amounts to a weak coupling

between the adaptation current and the spike generator. Its validity depends on the particular dynamics of the spike generator and the strength of the adaptation current, as stronger adaptation currents will also have stronger fluctuations. The potential dependence of the  $\gamma(f)$  term in equation 3.1a on  $A$  can be used to verify this assumption (see section 4).

In the appendix, we show that for small adaptation strength, the weight  $w$  in equation 3.6 is directly related to the neuron's normalized response function. Response functions are typically small during spikes and deviate strongly from zero between spikes (Reyes & Fetz, 1993; Hansel, Mato, & Meunier, 1995; Ermentrout, 1996). Strong fluctuations of the adaptation current during a spike and during the refractory period, as in Figure 3D, have almost no effect on the firing behavior. What really matters for spike generation is the time course of the adaptation current once the neuron has recovered from the last action potential.

Since in equation 3.7 we average over the variables  $V$ ,  $m$ , and  $h$  of the fast spike-generating dynamics, the detailed time course of these fast variables is no longer important. Due to the weak coupling assumption, their time course is independent of adaptation and thus is uniquely characterized by the resulting firing frequency, since usually the superthreshold part of  $f$ - $I$  curves is strictly monotonic. We can therefore replace the remaining term  $\langle m^p h^q (V - E_A) \rangle_{T,w}$  from averaging equation 2.1a by some function  $\tilde{\rho}(f)$ :

$$\langle m^p h^q (V - E_A) \rangle_{T,w} \approx \tilde{\rho}(f). \quad (3.8)$$

The example shown in Figure 4A illustrates how the time course of the voltage trace may depend on  $f$ . Similar graphs from experimental data can be found in the literature (see, e.g., Schwindt, 1973). To emphasize the functional form of  $\tilde{\rho}(f)$ , we rewrite this term as  $\rho \cdot [1 + \gamma(f)]$ , where  $\rho$  is a constant and  $\gamma(f)$  captures the frequency dependence (see Figure 4B).

The adaptation current can thus be approximated by a function depending only on  $f$ :

$$I_A \approx \bar{g}_A c(a)_{T\rho} \cdot [1 + \gamma(f)]. \quad (3.9)$$

For adaptation based on potassium currents (M-type and mAHP-type currents), both  $\rho$ , which equals  $\langle V - E_K \rangle_{T,w}$ , and  $c$  are positive. For slow recovery from inactivation of sodium currents where  $c < 0$ , the membrane potential stays always below the reversal potential  $E_{Na}$ , resulting in a negative  $\rho$ . Thus,  $c\rho$  is again positive. Defining

$$A := \bar{g}_M c(a)_{T\rho} \quad (3.10)$$

as the adaptation state  $A$  and inserting equation 3.9 into equation 3.4, we finally obtain equation 3.1a. Adaptation shifts the onset  $f$ - $I$  curve  $f_0(I)$ , as expected from equation 3.4. The  $\gamma(f)$  term adds a complication in that it distorts the  $f$ - $I$  curve.

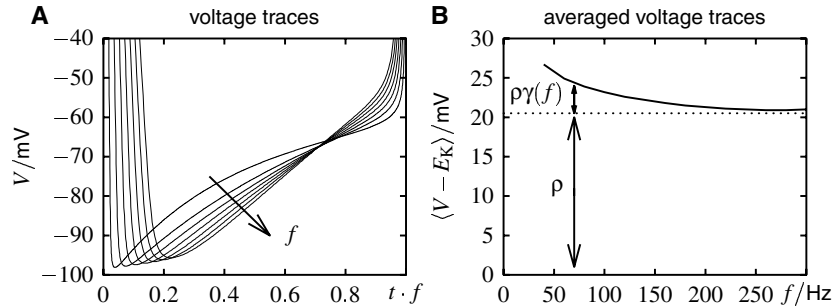


Figure 4: Averaging the membrane potential. (A) Time course of the membrane potential  $V(t)$  during interspike intervals for different firing frequencies  $f = 40, 80, 120, 160, 200, 240,$  and  $280$  Hz. Shown are results from the modified Traub-Miles model with mAHP-type current. For low firing frequencies, the membrane potential stays longer near about  $-70$  mV. With increasing firing frequency, more time is spent at more hyperpolarized potentials. (B) According to equation 3.8, the averaged driving force  $\langle V - E_K \rangle_{T,w}$  is a function of the firing frequency (for simplicity, we used the response function of the  $\theta$  neuron  $z(t) = 1 - \cos(2\pi t/T)$ ; Ermentrout, 1996) for the weight  $w$  to generate the data shown in the plot). Its absolute value  $\rho$  is larger than the  $f$ -dependent term  $\rho\gamma(f)$ .

**3.3 Averaging the Adaptation Dynamics.** It remains to show how the dynamics (3.1b) for the adaptation state  $A$  can be derived from the dynamics (2.1b) of the adaptation variable  $a$ . To do so, we average equation 2.1b over one ISI to get an equation for  $\langle a \rangle_T$ , which by definition, equation 3.10, is proportional to  $A$ .

The possible  $V$  dependence of  $\tau_a(V)$  introduces a complication. If we average equation (2.1b) directly, we have to factorize  $\langle \tau_a(V) da/dt \rangle_T$  into the product of  $\langle \tau_a(V) \rangle_T$  and  $\langle da/dt \rangle_T$  to isolate  $\langle a \rangle_T$ . However, this poses a problem as  $\tau_a(V)$  and  $da/dt$  co-vary. According to the Hodgkin-Huxley formalism,  $\tau_a(V)$  is given by  $a_\infty(V)$  divided by the corresponding rate constant  $\alpha(V)$  of the transition of the channels from their closed to their open state (Johnston & Wu, 1997). Typically,  $\alpha(V)$  increases monotonically, and  $a_\infty(V)$  is a sigmoidal function whose linear range is located above the cell's resting potential and  $\tau_a(V)$  takes its maximum above but close to the resting potential (see also Figure 2). This results in a brief but strong negative deflection of  $\tau_a(V)$  from its mean value during an action potential, as visible in Figure 3E. At the same time,  $a(t)$  increases in a step-like manner when a spike occurs. This implies that  $\tau_a(V)$  and  $da/dt$  are strongly anticorrelated. For example, for the Crook model displayed in Figure 3, the correlation is  $r = -0.79$ . Thus, we cannot average equation 2.1b directly and have to search for an alternative approach.

To isolate  $\langle a \rangle_T$ , we divide both sides of equation 2.1b by  $\tau_a(V)$  and then average over one ISI:

$$\left\langle \frac{da}{dt} \right\rangle_T = \left\langle \frac{a_\infty(V)}{\tau_a(V)} \right\rangle_T - \left\langle \frac{a}{\tau_a(V)} \right\rangle_T. \quad (3.11)$$

In general, the length of the averaging window  $T(t)$  depends on time  $t$ , so that

$$\left\langle \frac{da}{dt} \right\rangle_T = \frac{d\langle a \rangle_T}{dt} - \frac{dT/dt}{T} \left( \frac{a(t+T/2) + a(t-T/2)}{2} - \langle a \rangle_T \right). \quad (3.12)$$

Since we assume that  $a$  changes little during one ISI, we can neglect the last term in parentheses and obtain

$$\left\langle \frac{da}{dt} \right\rangle_T \approx \frac{d\langle a \rangle_T}{dt}. \quad (3.13)$$

We still have to replace the term  $\langle a/\tau_a(V) \rangle_T$  by an appropriate factorization. This is possible because the fast fluctuations of  $\tau_a(t)$  during a spike strongly reduce a possible correlation between  $a(t)$  and  $1/\tau_a(t)$ . In the simulation shown in Figure 3, this correlation is less than 0.15. The term  $\langle a/\tau_a(V) \rangle_T$  may therefore be approximated by  $\langle a \rangle_T \langle 1/\tau_a(V) \rangle_T$ .

Dividing equation 3.11 by  $\langle 1/\tau_a(V) \rangle_T$  then results in the desired dynamics for  $\langle a \rangle_T$ :

$$\frac{1}{\langle 1/\tau_a(V) \rangle_T} \frac{d\langle a \rangle_T}{dt} = \frac{1}{\langle 1/\tau_a(V) \rangle_T} \left\langle \frac{a_\infty(V)}{\tau_a(V)} \right\rangle_T - \langle a \rangle_T. \quad (3.14)$$

As shown for equation 3.8, we can approximate averages of functions depending on  $V$  by functions depending on the firing frequency  $f$ . Doing so, we obtain the time constant

$$\tilde{\tau}(f) \approx \frac{1}{\langle 1/\tau_a(V) \rangle_T} \quad (3.15)$$

and steady-state variable

$$\kappa(f) \approx \frac{1}{\langle 1/\tau_a(V) \rangle_T} \left\langle \frac{a_\infty(V)}{\tau_a(V)} \right\rangle_T. \quad (3.16)$$

With these abbreviations, equation 3.14 reads

$$\tilde{\tau}(f) \frac{d\langle a \rangle_T}{dt} = \kappa(f) - \langle a \rangle_T. \quad (3.17)$$

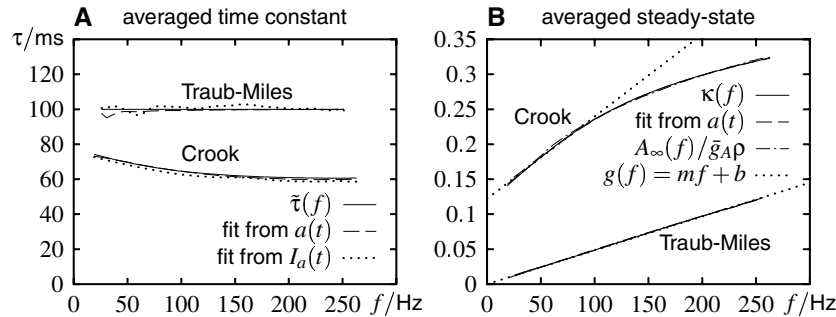


Figure 5: Averaging the dynamics of M-type current gating variables. Carrying out the same simulation as in Figure 3 (M-type current not included in the membrane equation) allows us to measure the adaptation time constant  $\bar{\tau}(f)$  and the steady-state variable  $\kappa(f)$  as a function of the firing frequency  $f$  from the time course of the gating variable  $a$ . Alternatively, these two quantities can be determined as the averages given in equations 3.15 and 3.16. The graphs show simulations of the modified Traub-Miles model and the Crook model. (A) The adaptation time constant as the average  $\bar{\tau}(f) = 1/\langle 1/\tau_a(V) \rangle_T$  over a single interspike interval (solid lines), fitted from the time course of the adaptation gating variable  $a(t)$  (dashed lines; see also Figure 3C), and fitted from the time course of the resulting adaptation current  $I_M$  (dotted lines; see also Figure 3D). All three measures agree well, thus confirming the averaging procedures. (B) The steady-state adaptation variable as the average  $\kappa(f) = 1/\langle 1/\tau_a \rangle_T \langle a_\infty/\tau_a \rangle_T$  over a single interspike interval (solid lines), measured from the time course of the adaptation gating variable  $a(t)$  (dashed lines), and as  $A_\infty(f)/\bar{g}_A\rho$  determined from the onset and steady-state  $f$ - $I$  curve of the models with the M-type current included using equation 4.2 (dashed-dotted lines). The factor  $\bar{g}_A\rho$  and the necessary offset were chosen to fit  $\kappa(f)$ . This resulted for the modified Traub-Miles model in  $\rho = 29$  mV and for the Crook model in  $\rho = 1.7$  mV. Again, all three measures agree well. For comparison, the best-fitting straight lines  $g(f) = mf + b$  for low firing frequencies are also plotted (dotted lines).

Both  $\kappa(f)$  and  $\bar{\tau}(f)$  can be obtained from either the time course of the adaptation gating variable  $a$  (see Figure 3C), or by the averages 3.15 and 3.16 over a single ISI. Both methods agree well, as illustrated in Figure 5 for the modified Traub-Miles model and the Crook model with M-type currents. It is worthwhile to compare  $\bar{\tau}(f)$  with the time constant governing  $\langle I_A \rangle_{T,w}$ . Figure 5A shows that these two functions agree well, too. Thus, at least for these two models and slowly varying input currents, the approximations involved in the averaging procedure are valid.

As suggested by Figure 5A, variations of  $\bar{\tau}(f)$  might be small compared to its absolute value. Therefore, we rewrite  $\bar{\tau}(f)$  as  $\tau[1 + \epsilon(f)]$  where  $\tau$  is a constant and  $\epsilon(f)$  captures the dependence on the firing frequency.

Multiplying equation 3.17 with  $\bar{g}_A c \rho$  and setting  $A_\infty(f) = \bar{g}_A c \rho \kappa(f)$ , we finally obtain the differential equation 3.1b for  $A = \bar{g}_A c \rho \langle a \rangle$  (equation 3.10).

#### 4 Parameters of the Adaptation Model

---

With the exception of the onset  $f$ - $I$  curve  $f_0(I)$ , all parameters of the model rely on microscopic properties of a specific adaptation mechanism through averages over the adaptation gating variable or the membrane potential. We next show how the model parameters can be obtained from macroscopic measurements.

**4.1 Steady-State Strength of Adaptation.** In steady state, the firing frequency is given by  $f_\infty(I)$ , and the adaptation state  $A$  equals  $A_\infty$ . Solving the equation for the adapted firing frequency (3.1a) for  $A_\infty$  results in

$$A_\infty(f_\infty) = \frac{I - f_0^{-1}(f_\infty)}{1 + \gamma(f_\infty)}, \quad (4.1)$$

where  $f_0^{-1}$  is the inverse function of the onset  $f$ - $I$  curve  $f_0$ . In steady state, the input  $I$  obeys  $I = f_\infty^{-1}(f_\infty)$ , so that

$$A_\infty(f) = \frac{f_\infty^{-1}(f) - f_0^{-1}(f)}{1 + \gamma(f)}. \quad (4.2)$$

In Figure 5B,  $A_\infty(f)$  is compared with the averaged steady-state gating variable  $\kappa(f)$ .

What functional behavior do we expect for  $A_\infty(f)$ ? Recall that  $A_\infty(f)$  is proportional to  $\kappa(f)$ . To understand the dependence of  $\kappa(f)$  on  $f$ , we decompose the time course of  $a_\infty(V(t))$  during one ISI into a stereotypical waveform  $a_S(t)$  reflecting the spike (with duration  $T_S$ ) and  $a_{ISI}(t)$  describing the nonspike-related part of  $a_\infty(V)$ . Assuming  $\tau_a(V)$  to be constant, the average equation 3.16, reads

$$\kappa(f) \approx \langle a_\infty(V) \rangle_T = \frac{1}{T} \left( \int_0^{T_S} a_S(t) dt + \int_0^T a_{ISI}(t) dt \right). \quad (4.3)$$

The first integral is a constant since the spike waveform is usually independent of firing frequency. The second integral is small compared to the first one since  $a_\infty(V)$  is not significantly activated by the low membrane potentials between spikes. We therefore expect  $\kappa(f)$ , and thus  $A_\infty(f)$ , to be proportional to  $f = 1/T$ . Deviations from this behavior are caused by an activation of adaptation channels between spikes, or by frequency-dependent spike deformations.

For the modified Traub-Miles model  $A_\infty(f)$  is indeed proportional to  $f$  (see Figure 5B), because the M-type current of this model is activated during spikes only (see Figure 2A). In the Crook model, however, the current is already activated at lower potentials. This causes a nonlinear  $\kappa(f)$  and a positive offset at  $f = 0$ . The offset can be removed by adding the spike-independent part of the M-type current to the membrane equation, 3.2. Doing so,  $\kappa(f)$  becomes approximately proportional to  $f$  for small firing frequencies.

**4.2 The  $\gamma(f)$  - Term.** The  $\gamma(f)$  term describes the frequency dependence of the averaged adaptation current, equation 3.9. To determine this term, at least one adapted  $f$ - $I$  curve  $f(I; A)$  of the neuron being at a certain constant adaptation state  $A$  is needed.  $\gamma(f)$  can then be derived from equation 3.1a,

$$\gamma(f) = \frac{I - f_0^{-1}(f(I; A))}{A} - 1. \quad (4.4)$$

In this equation,  $A$  is the distance between the onset  $f$ - $I$  curve  $f_0(I)$  and the adapted  $f$ - $I$  curve  $f(I; A)$  at some firing frequency. Note that  $\gamma(f)$  is small in a region around this firing frequency. It can therefore be neglected for small fluctuations of the input  $I$ . In Figure 6, an example of  $\gamma(f)$  is shown, together with information about how to measure  $f(I; A)$ .

Can we neglect the  $\gamma(f)$ -term if the input has larger fluctuations? Let us decompose the time course of the membrane potential into a stereotypical spike waveform  $V_S(t)$  of duration  $T_S$  and a second term  $V_{ISI}(t)$  describing the nonspike-related part of  $V$ . Similarly to equation 4.3, the average 3.8 with  $p = q = 0$  then reads

$$\begin{aligned} \tilde{\rho}(f) &= \langle V - E_A \rangle_{T,w} \\ &= \frac{1}{T} \left( \int_0^{T_S} \tilde{w}(t) V_S(t) dt + \int_0^T \tilde{w}(t) V_{ISI}(t) dt \right) - E_A. \end{aligned} \quad (4.5)$$

As a simplifying hypothesis, let us further assume that  $V_{ISI}(t)$ , as well as the weight function  $w(t)$ , obey a scale invariance such that  $V_{ISI}(t) = \hat{V}_{ISI}(tf)$  and  $w(t) = \hat{w}(tf)$ . Substituting  $x$  for  $tf$ , we get

$$\tilde{\rho}(f) \approx \frac{1}{T} \int_0^{T_S} w(t) V_S(t) dt + \int_0^1 \hat{w}(x) \hat{V}_{ISI}(x) dx - E_A. \quad (4.6)$$

The first integral covers spike-related phenomena and can be neglected because  $w(t)$  is small during the spike and usually  $T_S \ll T$ . According to our assumption, the second integral is independent of  $f$ , so that  $\tilde{\rho}(f)$  is constant. Thus, for this scenario, the  $\gamma(f)$  term vanishes. A nonzero  $\gamma(f)$

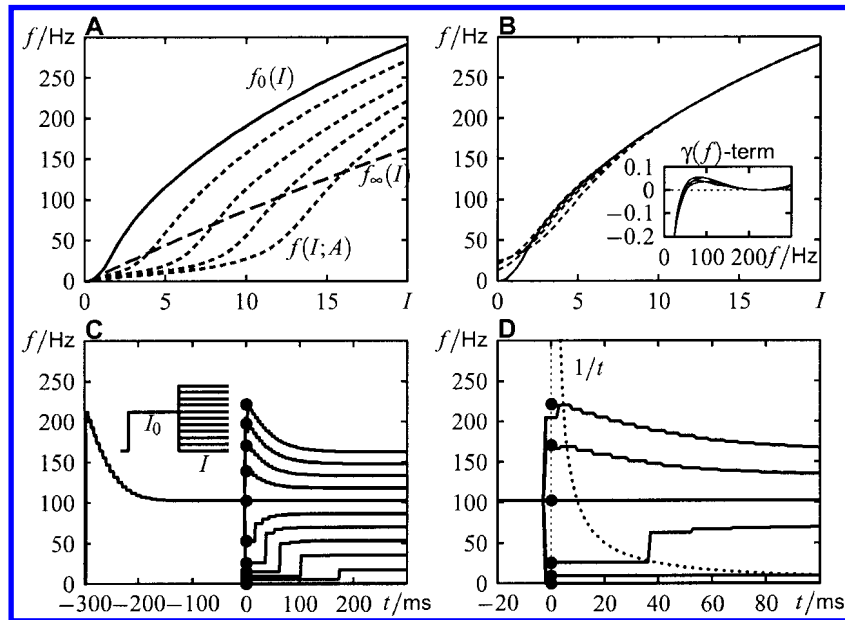


Figure 6: Adapted  $f$ - $I$  curves. (A) Comparison of some adapted  $f$ - $I$  curves  $f(I; A)$  with the onset  $f$ - $I$  curve  $f_0(I) \equiv f(I; 0)$  and the steady-state  $f$ - $I$  curve  $f_\infty(I) \equiv f(I; \infty)$  for the modified Traub-Miles with mAHP current. (B) The adapted  $f$ - $I$  curves shifted on top of the onset  $f$ - $I$  curve so that they align at  $f = 230$  Hz. As expected, all of these  $f$ - $I$  curves are similar in shape. The inset shows the corresponding  $\gamma(f)$  terms which were computed using equation 4.4 and the value of  $A$  set to the distance of the  $f$ - $I$  curves at  $f = 230$  Hz. The  $\gamma(f)$  terms are very similar, thus verifying the weak coupling assumption of the universal model. Above a firing frequency of approximately 50 Hz, the  $\gamma(f)$  term is small (less than 6%). The deviations of the  $f$ - $I$  curves and thus the high (negative) values of the  $\gamma(f)$ -term below 50 Hz may arise due to the difficulties in measuring the adapted  $f$ - $I$  curves. (C) Firing frequencies evoked by the protocol for measuring an adapted  $f$ - $I$  curve (see the inset). In this example, the neuron is first adapted to  $I_0 = 12$  (conditioning stimulus,  $-300 \text{ ms} < t < 0$ ). Then the input is stepped to different test stimuli  $I$  ( $t > 0$ ) to measure the initial response of the adapted neuron at these intensities (dots). The responses to higher test intensities show sharp peaks, which decay back to a new steady state. Lower test intensities result in decreased responses, which increase due to recovery from adaptation to the corresponding steady-state values. (D) A closer look at some of the responses in C reveals that the initial responses for stimulus intensities below the conditioning stimulus are not well defined. Since the neuron responds with repetitive firing to the conditioning stimulus, there might be a spike at  $t = 0$  or shortly before. Thus, the lowest firing frequency that can be measured before a spike at time  $t$  is  $f \approx 1/t$  (dotted line). As a consequence, firing frequencies (dots) measured below the  $1/t$  line overestimate the real response. This results in the tails of the adapted  $f$ - $I$  curves in A.

term most likely results from a dependence of  $V_{ISI}(t)$  on  $f$ , which does not scale with  $f$ . Figure 4 gives one example.

Note that the  $\gamma(f)$  term should be independent of  $A$  (see the inset in Figure 6B). If this is not the case, then the weak coupling assumption of the model is invalid.

**4.3 Time Constants of Adaptation.** In addition to the onset  $f$ - $I$  curve, the steady-state  $f$ - $I$  curve, and the  $\gamma(f)$  term, we still need to know how to measure the adaptation time constant  $\tau$  in equation 3.1b in order to apply the adaptation model to experimental data. To address this issue, we explore the relation between  $\tau$  and the effective time constant  $\tau_{\text{eff}}$  describing the decay of the firing frequency during constant stimulation (see Figure 1B). First, we discuss why these two time constants differ in general. Then we investigate how the time course of the adaptation state can be measured and used to estimate  $\tau$ . Finally, we linearize the model 3.1 to give a direct relation between  $\tau$  and  $\tau_{\text{eff}}$ .

The different estimates of  $\tau$  are illustrated in Figure 7. For simplicity, the  $\epsilon(f)$  term introducing a dependence of the adaptation time constant on the firing frequency is neglected in the following analysis. We justify this in the last paragraph of this section.

In general, the adaptation time constant  $\tau$  is not identical with the effective time constant  $\tau_{\text{eff}}$  (see Figure 1D). The main reason is that the steady-state strength of adaptation  $A_\infty$  depends on the actual firing frequency. Thus,  $A_\infty$  is not constant, and  $A(t)$  is not necessarily an exponential function with time constant  $\tau$ . The time constant  $\tau_A$ , which we obtain by fitting a single exponential to the time course of  $A(t)$ , may therefore differ from  $\tau$ . A possible discrepancy between  $\tau$  and  $\tau_{\text{eff}}$  may also be due to the onset  $f$ - $I$  curve and the  $\gamma(f)$  term. Both determine how  $A$  influences  $f$ . If  $\gamma(f)$  is nonzero or the onset  $f$ - $I$  curve is nonlinear,  $\tau_{\text{eff}}$  differs from  $\tau_A$  and thus from  $\tau$ .

Knowing  $f_0(I)$  and  $\gamma(f)$  enables one to calculate the time course of  $A$  from equation 3.1a:

$$A = \frac{I - f_0^{-1}(f)}{1 + \gamma(f)}. \quad (4.7)$$

Using this equation, the time evolution of  $A$  can be computed without any knowledge about the adaptation time constant and mechanism, provided  $f_0^{-1}(I)$  exists. This is guaranteed if  $f_0(I)$  is strictly monotone in the region of interest but excludes the subthreshold region where  $f_0(I)$  vanishes. From the decay of  $A$  for constant  $I$ , the corresponding time constant  $\tau_A$  can be obtained by fitting a single exponential on  $A(t)$ .

The dependence of  $A_\infty$  on  $f$  still causes  $\tau_A$  to differ from  $\tau$ . However, for subthreshold stimuli,  $f$  is zero and so is  $A_\infty$ . Equation 3.1b reduces to  $\tau dA/dt = -A$ , an exponential recovery of  $A$  with time constant  $\tau$ . Since

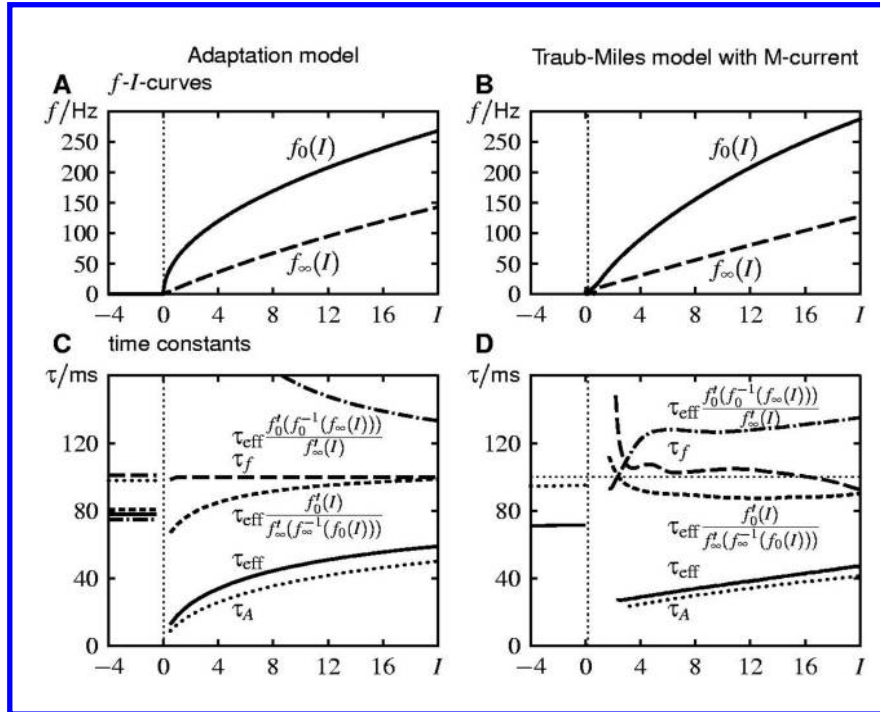


Figure 7: Adaptation time constants. (A) The onset  $f$ - $I$  curve and the steady-state  $f$ - $I$  curve used for the simulation of time constants shown in C. The choice  $f_0(I) = 60\sqrt{I}$  reproduces the shape of a typical  $f$ - $I$  curve of a type I neuron (Ermentrout, 1996) and the corresponding steady-state  $f$ - $I$  curve  $f_\infty(I) = 60\sqrt{I + 0.1^2 60^2/4} - 0.1 \cdot 60^2/2$  results from linear adaptation of medium strength with  $A_\infty(f) = 0.1 \cdot f$ . (B) The  $f$ - $I$  curves of the modified Traub-Miles model with M-type current as a more realistic example for estimating the adaptation time constant. (C) Time constants calculated from  $f(t)$  simulated with the model 3.1 using the  $f$ - $I$  curves shown in A and  $\tau = 100$  ms. (D) Time constants resulting from simulations with the Traub-Miles model where  $\tau = 100$  ms (horizontal dotted line). (C, D) For subthreshold stimuli ( $I < 0$ ), the time constants were derived from recovery from adaptation, as explained in the text. For superthreshold stimuli,  $\tau_{\text{eff}}$  is directly measured from  $f(t)$  by means of an exponential fit. For sub- and especially superthreshold stimuli,  $\tau_{\text{eff}}$  is smaller than  $\tau$ . The time constant  $\tau_A$  of the decay of  $A(t)$  was computed from the response  $f(t)$  using equation 4.7. For superthreshold stimuli,  $\tau_A$  differs clearly from  $\tau$ . The correction of  $\tau_{\text{eff}}$  with  $f'_0(f_0^{-1}(f_\infty(I)))/f'_\infty(I)$  overestimates  $\tau$ , whereas the correction with  $f'_0(I)/f'_\infty(f_\infty^{-1}(f_0(I)))$  results in values much closer to  $\tau$ . An alternative way to estimate  $\tau$  is to fit  $f(t)$  computed with the model 3.1 to the measured  $f(t)$  with  $\tau$  as the fit parameter. This gives the best estimate  $\tau_f$  of the true  $\tau$ . For subthreshold stimulus intensities,  $\tau_A$  reveals a good estimate of  $\tau$  too. (D) Note that for low firing frequencies (at about  $I < 4$ ), the model assumption  $f \gg 1/\tau$  is not fulfilled.

$f = 0$ , we cannot compute the time course of  $A$  directly from equation 4.7. Instead, we have to probe  $A(t)$  by applying short test stimuli with given intensity  $I$  at different times after the offset of an adaptation stimulus. From the onset firing frequencies evoked by these stimuli, we can infer  $A(t)$  through equation 4.7. By fitting a single exponential on  $A(t)$ , we finally obtain  $\tau$ . Note, however, that with this method, we violate the assumption of high firing frequencies. For  $V$ -dependent time constants  $\tau_n(V)$ , like the one of the M-type current in the Crook model (see Figure 2B), this method measures the value of the time constant at resting potential, which can be much smaller than  $\tau$  for the superthreshold regime.

A simple method to estimate  $\tau$  for the superthreshold regime is to calculate it directly from  $\tau_{\text{eff}}$ . Eliminating  $A$  in equation 3.1b using equations 3.1a and 4.2, and expanding the  $f$ - $I$  curves around  $f_\infty(I)$ ,

$$f_\infty^{-1}(f) \approx I + \left. \frac{df_\infty^{-1}}{df} \right|_{f=f_\infty(I)} \cdot (f - f_\infty(I)) \quad (4.8a)$$

$$f_0^{-1}(f) \approx f_0^{-1}(f_\infty(I)) + \left. \frac{df_0^{-1}}{df} \right|_{f=f_\infty(I)} \cdot (f - f_\infty(I)), \quad (4.8b)$$

results in a linear differential equation for  $f$ :

$$\tau_{\text{eff}}(I) \frac{df}{dt} = f_\infty(I) + \tau_{\text{eff}}(I) f_0'(f_0^{-1}(f_\infty(I))) \frac{dI}{dt} - f. \quad (4.9)$$

In this equation,  $\tau_{\text{eff}}$  is the decay constant of the firing frequency  $f$ , which is given by

$$\tau_{\text{eff}}(I) = \tau \frac{f_\infty'(I)}{f_0'(f_0^{-1}(f_\infty(I)))}. \quad (4.10)$$

Thus,  $\tau$  is scaled by the slopes of the  $f$ - $I$  curves at the steady-state frequency  $f_\infty(I)$ .

This approximation is correct for small deviations of  $f$  from  $f_\infty(I)$ . However,  $\tau_{\text{eff}}$  is usually measured by applying a constant stimulus to the unadapted neuron, as in Figure 1. In this case, the initial response deviates significantly from the steady state and dominates the estimate of  $\tau_{\text{eff}}$ . It might therefore be better to expand the  $f$ - $I$  curves at  $f_0(I)$  instead of  $f_\infty(I)$ . Doing so, we get

$$\tau_{\text{eff}}(I) = \tau \frac{f_\infty'(f_\infty^{-1}(f_0(I)))}{f_0'(I)}, \quad (4.11)$$

which generalizes the results of Ermentrout (1998) to arbitrary  $f$ - $I$  curves. Especially slightly above the firing threshold of the onset  $f$ - $I$  curve  $f_0(I)$ , its

slope is much larger than that of the steady-state  $f$ - $I$  curve. This causes  $\tau_{\text{eff}}$  to be smaller than at higher input intensities. However, the time constant resulting from the M-type current of the Crook model (see Figure 5A) increases for small  $f$ , thus counteracting the effect of the  $f$ - $I$  curves. Inverting equation 4.11 allows us to estimate the adaptation time constant  $\tau$  from the measured  $\tau_{\text{eff}}$ , as illustrated in Figure 7.

An alternative and more precise method to estimate  $\tau$  is to fit  $f(t)$  computed with the model 3.1 to the measured  $f(t)$  with  $\tau$  as the fit parameter. If the resulting  $\tau$  depends strongly on the input, one might consider the possible dependence of the time constant on  $f$ ; that is,  $\epsilon(f)$  may not be negligible.

How strongly might  $\tilde{\tau}(f)$  depend on  $f$ ? By definition 3.15, the answer is determined by how  $V(t)$  depends on  $f$ . This is similar to the  $f$  dependence arising from averaging the driving force  $V - E_A$ , equation 3.8, discussed earlier (see equation 4.6 and Figure 4) with the difference that now the average is not weighted by  $w$ . Since spikes are short compared to the remaining ISI, the main contribution of a possible dependence of  $\tilde{\tau}(f)$  on  $f$  results from changes of the time course of  $V_{\text{ISI}}(t)$ , which cannot be explained by a simple scaling in time by  $f$ . Thus, we expect  $\tilde{\tau}(f)$  to depend only weakly on  $f$ . The Crook model (see Figure 5A) confirms this expectation. For firing frequencies higher than 100 Hz, it reaches a constant value. However, for lower firing frequencies, it depends on  $f$ . On the other hand, the time constant of the modified Traub-Miles model is constant by definition.

## 5 Signal-Transmission Properties

---

Using the phenomenological model, equation 3.1, we can now quantify the influence of adaptation on the signal transmission properties of a neuron based solely on the knowledge of its  $f$ - $I$  curves and adaptation time constant. Formulating filter properties of a neuron in terms of  $f$ - $I$  curves has the important advantage that they can easily be measured with standard current injection techniques. This allows quantifying functional properties of individual neurons with low experimental effort.

There are two different types of  $f$ - $I$  curves that have to be distinguished when discussing the signal-transmission properties of a neuron that exhibits adaptation: the adapted  $f$ - $I$  curves  $f(I; A)$  including the onset  $f$ - $I$  curve  $f_0(I) = f(I; 0)$  as a special case, on the one hand, and the steady-state  $f$ - $I$  curve  $f_\infty(I)$ , on the other hand. In Figure 6A, these different  $f$ - $I$  curves are illustrated for the modified Traub-Miles model. The adapted  $f$ - $I$  curves describe the instantaneous response of a neuron in a given and fixed adaptation state  $A$ . They are important for the transmission of stimulus components, which are faster than the adaptation dynamics, since only for such stimuli, the adaptation state can be considered to be fixed (for more details, see section 5.3). Second, there is the steady-state  $f$ - $I$  curve  $f_\infty(I)$ . It describes the response of the neuron when it is fully adapted to the ap-

plied fixed stimulus intensity and is therefore the relevant  $f$ - $I$  curve for the transmission of stimulus components slower than the adaptation dynamics.

**5.1 Adapted  $f$ - $I$  Curves.** What do the  $f$ - $I$  curves  $f(I; A)$  look like? Neglecting the  $\gamma(f)$  term, equation (3.1a) simplifies to  $f = f_0(I - A)$ . For fixed  $A$ , the adapted  $f$ - $I$  curves are thus obtained by shifting the onset  $f$ - $I$  curve by  $A$ . Adapted  $f$ - $I$  curves of the modified Traub-Miles model (see Figure 6A) indeed align on top of the onset  $f$ - $I$  curve (see Figure 6B).

We measure adapted  $f$ - $I$  curves by first applying a constant stimulus  $I_0$  to prepare the neuron in a specific adaptation state  $A$ . We then use different test intensities  $I$  and construct the adapted  $f$ - $I$  curve from the evoked onset firing frequencies (see Figures 6C and 6D).

**5.2 Linear Steady-State  $f$ - $I$  Curves and Linear Adaptation.** Alternatively, we can ask which functional form the steady-state  $f$ - $I$  curve  $f_\infty(I)$  has, given a specific dependence of  $A_\infty$  on  $f$ . As shown by Ermentrout (1998), adaptation linearizes the  $f_\infty(I)$ -curve. We now generalize his analysis.

In steady state,  $f$  equals  $f_\infty(I)$  and  $A = A_\infty$ . From equation 3.1a, we obtain the implicit equation

$$f_\infty(I) = f_0(I - A_\infty(f_\infty(I)) \cdot [1 + \gamma(f_\infty(I))]). \quad (5.1)$$

This equation can be generalized if  $A$  acts through a function  $\eta(A)$ . For example, an AHP-type current may depend nonlinearly on the calcium concentration, which represents the adaptation state. The implicit equation for  $f_\infty(I)$  then reads

$$\begin{aligned} f_\infty(I) &= f_0(I - \eta(A_\infty(f_\infty(I))) \cdot [1 + \gamma(f_\infty(I))]) \\ &=: f_0(I - \tilde{I}_A(f_\infty(I))). \end{aligned} \quad (5.2)$$

$\tilde{I}_A(f) := \eta(A_\infty(f)) \cdot [1 + \gamma(f)]$  generalizes the averaged steady-state adaptation current. Differentiating both sides of equation 5.2 yields

$$\frac{df_\infty(I)}{dI} = f_0'(I - \tilde{I}_A(f_\infty(I))) \cdot \left(1 - \tilde{I}'_A(f_\infty(I)) \frac{df_\infty(I)}{dI}\right), \quad (5.3)$$

where the prime denotes a derivative with respect to the argument. We obtain

$$\tilde{I}'_A(f_\infty(I)) = \frac{1}{f_\infty'(I)} - \frac{1}{f_0'(I - \tilde{I}_A(f_\infty(I)))}. \quad (5.4)$$

There are two possibilities to obtain a linear steady-state  $f$ - $I$  curve.

First, the derivative of the onset  $f$ - $I$  curve is either constant or infinity. The latter is true for type I neurons, whose onset  $f$ - $I$  curve is a square root function near their threshold (Ermentrout, 1996). The derivative of  $\tilde{I}_A$  then also has to be constant. This implies that  $\tilde{I}_A$  is allowed to vary only linearly with  $f$ . This is the case if  $\gamma(f)$  vanishes and if  $\eta(A_\infty(f))$  depends linearly on  $f$ . Since most likely  $A_\infty$  is already proportional to the firing frequency (see Figure 5B),  $\eta(A)$  has to equal  $A$ . We thus obtain

$$\tilde{I}_A(f_\infty) = m \cdot f_\infty, \tag{5.5}$$

where  $m$  is a proportionality constant. We refer to this set of conditions as linear adaptation, since if they are satisfied,  $\tilde{I}_A$  as well as  $A_\infty$  depend linearly on  $f$ . Thus, linear adaptation guarantees a linear steady-state  $f$ - $I$  curve for a linear or very steep onset  $f$ - $I$  curve. See Figures 8 and 9B for illustrations.

The second possibility is that the derivative of the onset  $f$ - $I$  curve is neither constant nor infinity. A linear steady-state  $f$ - $I$  curve then can still arise if the  $\tilde{I}_A$  fulfills equation 5.4 with  $f'_\infty(I) = \text{const}$  and  $f'_0(I)$  calculated from the observed onset  $f$ - $I$  curve. We conclude that adaptation may (but need not) linearize the steady-state  $f$ - $I$  curve.

In the same manner, we can examine the influence of the  $\gamma(f)$  term on the adapted  $f$ - $I$ -curves. Since  $A$  is fixed, the only term introducing an  $f$

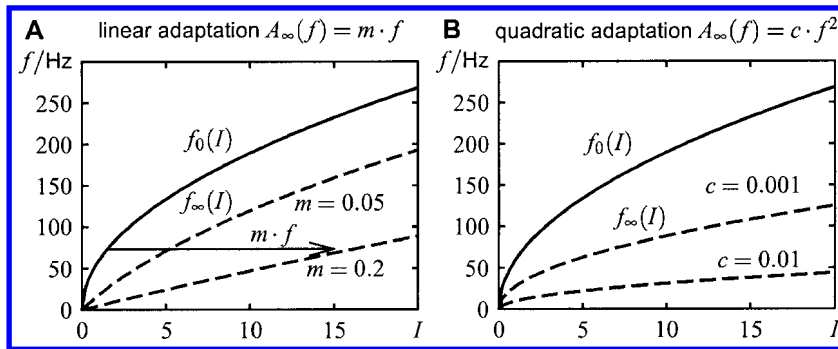


Figure 8: Linearization of the steady-state  $f$ - $I$  curve. The effect of adaptation on an onset  $f$ - $I$  curve given by  $f_0(I) = 60\sqrt{I}$  is shown for  $\gamma(f) = 0$  and  $\eta(A) = A$ . (A) Linear adaptation  $A_\infty(f) = m \cdot f$  linearizes and compresses the steady-state  $f$ - $I$  curve. The steady-state  $f$ - $I$  curve is approximately linear as long as the firing frequency is so small that the onset  $f$ - $I$  curve is close to a vertical line. Adaptation maps each point of the onset  $f$ - $I$  curve to the steady-state  $f$ - $I$  curve by shifting it by the adaptation strength  $A_\infty(f)$  to higher input values as sketched by the arrow. (B) With quadratic adaptation  $A_\infty(f) = c \cdot f^2$ , the steady-state  $f$ - $I$  curves are downscaled versions of the onset  $f$ - $I$  curve. This type of adaptation therefore does not linearize  $f_\infty(I)$ .

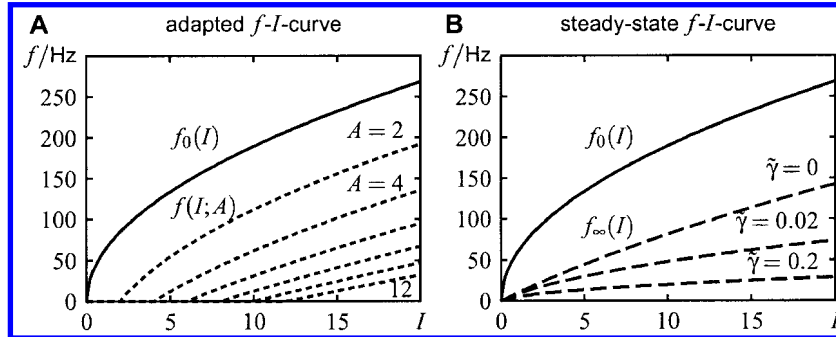


Figure 9: Influence of the  $\gamma(f)$  term on  $f$ - $I$  curves. (A) With linear  $\gamma(f) = 0.02f$  and increasing adaptation  $A = 2, 4, 6, 8, 10, 12$ , the adapted  $f$ - $I$  curves  $f(I; A)$  are linearized and compressed. (B) The linearizing effect of linear adaptation  $A_\infty(f) = 0.1f$  on the steady-state  $f$ - $I$  curve  $f_\infty(I)$  is destroyed by a linear  $\gamma(f)$  term ( $\gamma(f) = \tilde{\gamma}f$ ,  $\tilde{\gamma} = 0, 0.02, 0.2$ ).

dependence is  $\gamma(f)$ :

$$f(I; A) = f_0(I - A \cdot [1 + \gamma(f)]). \quad (5.6)$$

Taking derivatives of both sides of this equation and rearranging terms results in

$$\gamma'(f)A = \frac{1}{f'(I; A)} - \frac{1}{f'_0(I - A \cdot [1 + \gamma(f)])}. \quad (5.7)$$

Analogous to the situation for  $f_\infty(I)$  (see equation 5.4), there are two cases for getting a linear adapted  $f$ - $I$  curve. First, if the onset  $f$ - $I$  curve is either a straight line or has an infinite slope at threshold, then  $\gamma(f)$  must depend linearly on  $f$  (see Figure 9). Note that in this scenario, linear steady-state  $f$ - $I$  curves are not possible. Second, if the onset  $f$ - $I$  curve is neither a straight line nor has an infinite slope, then the  $\gamma(f)$  term must depend appropriately on  $f$  according to equation 5.7 with  $f'(I; A)$  only depending on  $A$ . In this case, linear steady-state  $f$ - $I$  curves are unlikely since at the same time,  $\gamma(f)$  and  $\tilde{I}_A$  have to satisfy equations 5.7 and 5.4, respectively.

From a different point of view, we may summarize these findings as follows, given a type I or linear onset  $f$ - $I$  curve. Observing a linearized steady-state  $f$ - $I$  curve implies that  $\gamma(f)$  can be neglected and that the averaged adaptation current  $\tilde{I}_A(f)$  depends linearly on  $f$ . A nonlinear steady-state  $f$ - $I$  curve implies a nontrivial  $\gamma(f)$  term or a nonlinear  $\tilde{I}_A(f)$ . If the adapted  $f$ - $I$  curves are shifted versions of the onset  $f$ - $I$  curve, the  $\gamma(f)$  term can be ruled out, and the nonlinear steady-state  $f$ - $I$  curve is caused by a nonlinear  $\tilde{I}_A(f)$ . Note, however, that if the slope of the onset  $f$ - $I$  curve is neither constant nor infinity, such general statements cannot be made.

**5.3 High-Pass Filter Properties Due to Adaptation.** Spike-frequency adaptation is responsible for high-pass filter properties, since adaptation currents resemble an inhibitory feedback. By means of the model 3.1, we can easily quantify these filter properties for a specific neuron from the knowledge of its onset and steady-state  $f$ - $I$  curve, and its adaptation time constant.

In essence, model 3.1 involves linear dynamics. The only nonlinearities are introduced by the  $f$ - $I$  curves and the  $\gamma(f)$  term. Consider a stimulus  $I(t)$  with sufficiently small fluctuations so that the  $f$ - $I$  curves can be linearized around the steady-state firing frequency and the  $\gamma(f)$  term can be neglected. We then obtain equation 4.9, which is linear in  $f$ , and we can calculate its transfer function  $H_f(\omega)$  by means of Fourier transformation.

$$|H_f(\omega)| = f'_\infty \sqrt{\frac{1 + (\omega\tau_{\text{eff}}f'_0/f'_\infty)^2}{1 + \omega^2\tau_{\text{eff}}^2}} \quad (5.8)$$

is the gain for each frequency component  $\omega/2\pi$  of the stimulus. Gain and phase shift of  $H_f$  are plotted in Figures 10A and 10B.

Mean and low-frequency components of the stimulus up to  $\omega\tau_{\text{eff}} \approx 0.2$  are transmitted via the slope of the steady-state  $f$ - $I$  curve ( $|H_f(0)| = f'_\infty$ ). Fast fluctuations with  $\omega\tau_{\text{eff}} > 2$  are transmitted much better by the slope of the onset  $f$ - $I$  curve ( $\lim_{\omega\tau_{\text{eff}} \rightarrow \infty} |H_f(\omega)| = f'_0$ ). In between, at around  $\omega_c\tau_{\text{eff}} = 1$ , the firing frequency response shows the strongest phase advance.

This high-pass frequency property of adaptation can be best understood by the dynamics 3.1b of the adaptation variable  $A$ . Substituting  $f$  in equation 4.2 for  $A_\infty$  by equation 3.1a, setting  $\gamma(f) = 0$ , and linearizing at  $f = f_\infty(I)$  results in

$$\tau_{\text{eff}} \frac{dA}{dt} = I(1 - f'_\infty/f'_0) - A. \quad (5.9)$$

The transfer function  $H_A(\omega)$  of this low-pass filter is shown in Figures 10C and 10D. The adaptation  $A$  follows directly the low-frequency components ( $\omega\tau_{\text{eff}} < 0.2$ ) of the stimulus, thus shifting the onset  $f$ - $I$  curve appropriately toward the corresponding values of the steady-state  $f$ - $I$  curve. As a consequence, these slow components are transmitted by the steady-state  $f$ - $I$  curve. High-frequency components ( $\omega\tau_{\text{eff}} > 2$ ) have almost no effect on  $A$ . Thus, fast components are transmitted by an adapted  $f$ - $I$  curve, which is the onset  $f$ - $I$  curve shifted to higher input intensities because of low-frequency components. The shift of the onset  $f$ - $I$  curve compensates for the mean value of the stimulus and optimizes the transmission of fast fluctuations, generating a special high-pass filter.

Note that the transfer functions of both  $f$  and  $A$  depend on the effective time constant  $\tau_{\text{eff}}$  and not on the adaptation time constant  $\tau$ .  $\tau_{\text{eff}}$  usually is a function of the input  $I$ , as shown in the context of Figure 7. This may

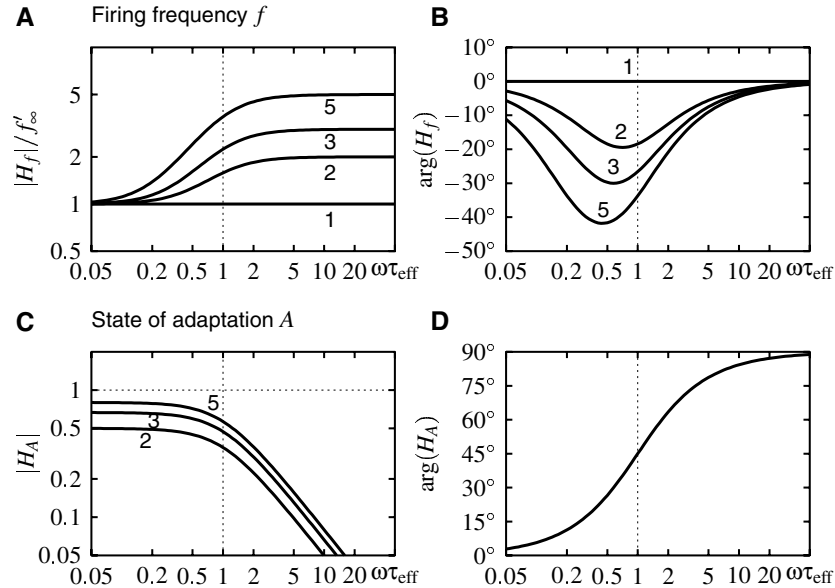


Figure 10: Transfer functions. (A) Gain and (B) phase shift of the transfer function for the firing frequency  $f(t)$ . The gain (see equation 5.8) is plotted as multiples of the slope  $f'_\infty$  of the steady-state  $f$ - $I$  curve. At negative phase shifts, the output firing frequency advances the input. (C) Gain and (D) phase shift of the transfer function for the adaptation state  $A(t)$  (see equation 5.9). The gain and the frequency axis are plotted logarithmically. For  $\tau_{\text{eff}} \approx 160$  ms, the values of the frequency axis correspond to frequency components measured in Hertz. The dotted vertical line marks the cut-off frequency at  $\omega\tau_{\text{eff}} = 1$ . The labels indicate the ratios  $f'_0/f'_\infty$  of the slopes of the  $f$ - $I$  curves.

result in cut-off frequencies much higher than expected from the value of the adaptation time constant. The dynamical behavior of an adapting neuron is therefore determined by the combined effects of the relative slopes of the onset and steady-state  $f$ - $I$  curves and the adaptation time constant  $\tau$ .

## 6 Combining Adaptation and Spike Generation

The model, equation 3.1, simply maps the stimulus  $I(t)$  through the onset  $f$ - $I$  curve  $f_0(I)$  into a firing frequency  $f(t)$  for a description of the spike generator. This approach is valid as long as the input current  $I(t)$  is approximately constant during an interspike interval.

As a consequence of this simple mapping,  $f(t)$  fluctuates as fast as  $I(t)$  does. However, the transformation of a stimulus into a sequence of spikes acts like a low-pass filter. Given the spikes only, fluctuations of the stimulus

$I(t)$  between two succeeding spikes cannot be observed. Thus, the firing frequency  $\nu(t)$  measured from the spikes as the reciprocal of the interspike intervals is in general different and varies more slowly than the model's  $f(t)$ . Only for stimuli that are approximately constant between two spikes,  $f(t)$  approaches  $\nu(t)$ .

For more rapidly varying stimuli,  $f(t)$  has to be fed into a model generating spikes from which a firing frequency  $\nu(t)$  can be calculated and compared with the firing frequency measured experimentally.

The simplest way to do this is to use a nonleaky phase oscillator. This is the canonical model of dynamical systems having a stable limit cycle, just like a spike generator in its superthreshold regime for constant stimuli (Hoppensteadt & Izhikevich, 1997). Here we apply it to time-dependent stimuli:

$$\begin{aligned} \frac{d\varphi}{dt} &= f(t); & \varphi < 1 \\ \varphi &= 0; & \varphi = 1 \rightarrow \text{spike} \end{aligned} \quad (6.1)$$

The activity  $f(t) = f_0(I - A[1 + \gamma(f)])$  from the adaptation model, equation 3.1, is the velocity of the phase angle  $\varphi$ . Every time  $\varphi$  reaches unity, a cycle is completed and a spike elicited.

We can also use the phase oscillator 6.1 to compute a continuous firing frequency  $\nu(t)$ . At each time  $t$ , we integrate the activity  $f$  symmetrically both backward and forward in time until the integral reaches the value one:

$$\int_{t-\frac{1}{2}T(t)}^{t+\frac{1}{2}T(t)} f(t') dt' = 1. \quad (6.2)$$

The reciprocal of the required integration time  $T$  is the desired firing frequency  $\nu(t)$ . Dividing this equation by  $T$  results in an implicit equation for  $\nu(t)$  as a running average with variable time window  $T(t) = 1/\nu(t)$ :

$$\nu(t) = \frac{1}{T(t)} \int_{t-\frac{1}{2}T(t)}^{t+\frac{1}{2}T(t)} f(t') dt'. \quad (6.3)$$

Computing  $\nu(t)$  using equation 6.2 captures a large fraction of the low-pass properties of a spiking neuron, but of course this is only a simple sketch of a real spike generator.

To extend our general approach to lower firing frequencies and stronger adaptation currents, it is necessary to incorporate the interaction between adaptation and spike generation. Let

$$\frac{d\vec{x}}{dt} = \vec{g}(\vec{x}, I(t)) \quad (6.4)$$

be the dynamics of a specific spike generator, that is, an  $N$ -dimensional system of differential equations, which is driven by the input current  $I(t)$ . Whenever one of the variables  $\vec{x}(t)$  (e.g., the membrane potential or a phase angle) crosses a threshold, there is a spike, and this variable may be reset. This is a general formulation of conductance-based models (see equation 3.2), integrate-and-fire models, and phase oscillators (such as equation 6.1). For the  $\theta$  model (Ermentrout, 1996), for example,  $\vec{x} = \theta$  and  $\vec{g}(\vec{x}, I(t)) = q(1 - \cos \theta) + (1 + \cos \theta)c(I(t) - I^*)$ , where  $q$  and  $c$  are constants and  $I^*$  is the input intensity at which the bifurcation from quiescence to repetitive firing occurs. Whenever the phase angle  $\theta$  crosses  $\pi$  there is a spike and  $\theta$  is reset to  $-\pi$ . In order to use the adaptation model, equation 3.1, in conjunction with equation 6.4, we need to go back to the general adaptation current, equation 2.1, by undoing the averages but keeping the parameterization.

An intermediate approach for moderate adaptation currents is

$$\frac{d\vec{x}}{dt} = \vec{g}(\vec{x}, I(t) - A(t) \cdot [1 + \gamma(\nu)]) \quad (6.5a)$$

$$\tau \cdot [1 + \epsilon(\nu)] \frac{dA}{dt} = \frac{A_\infty(\nu)}{\nu} \delta(t - t_i) - A, \quad (6.5b)$$

where  $\delta(t - t_i)$  is Dirac's delta function,  $t_i$  is the time of the last spike, and  $\nu = 1/(t_i - t_{i-1})$  is the instantaneous firing frequency. For the  $\theta$  model example, this equation reads

$$\frac{d\theta}{dt} = q(1 - \cos \theta) + (1 + \cos \theta)c(I - A - I^*) \quad (6.6a)$$

$$\tau \frac{dA}{dt} = s\delta(t - t_i) - A, \quad (6.6b)$$

where we set  $\gamma(\nu) = 0$ ,  $\epsilon(\nu) = 0$ , and  $A_\infty(\nu)/\nu = s = \text{const}$  to emphasize the linear character of such an adaptation current. All parameters  $\gamma$ ,  $\tau$ ,  $\epsilon$ , and  $A_\infty$  of the adaptation current in equations 6.5 and 6.6 are equal to those of the universal model, 3.1, and thus can be easily measured. However, a model like 6.5 is still limited to adaptation that is weakly coupled to the spike generator.

To overcome this limitation, we have to give up the independence of the adaptation model from microscopic properties of specific adaptation mechanisms. Consider

$$\frac{d\vec{x}}{dt} = \vec{g}(\vec{x}, I(t) - y \cdot \tilde{\rho}(\vec{x})) \quad (6.7a)$$

$$\tau \cdot [1 + \epsilon(\nu)] \frac{dy}{dt} = \frac{y_\infty(\nu)}{\nu} \delta(t - t_i) - y. \quad (6.7b)$$

The adaptation variable  $y = \tilde{g}_A c a$  is proportional to the adaptation gating variable  $a$ .  $\tilde{\rho}(\vec{x}) = m^p h^q (V - E_A)$  covers the coupling of the adaptation cur-

rent on the variables  $\vec{x} = (V, m, h, \dots)$  of the spike generator. This term is no longer independent of the adaptation mechanism. If adaptation is caused by slow recovery from inactivation, then  $p > 0$  or  $q > 0$ . For all other adaptation mechanisms,  $p = q = 0$ . The adaptation reversal potential  $E_A$  is an additional free parameter. Future studies will show which phenomenological quantities measure this parameter.

The parameterization with macroscopically measurable quantities makes equations 6.5 and probably 6.7 superior to using a standard adaptation current like the M-type current, since all parameters can be estimated from measurements of the firing frequency without the knowledge of the specific adaptation mechanism.

## 7 Discussion

---

Based on a thorough mathematical analysis of several basic spike adaptation mechanisms, a universal phenomenological adaptation model, 3.1, has been introduced in this article. Our approach combines three important aspects: biophysics of ionic currents, electrophysiology, and the theory of signal processing. First, the model is derived from well-known biophysical kinetics. Second, the model is completely defined by macroscopic quantities such as the neuron's  $f$ - $I$  curves and the adaptation time constant. These can be measured easily with standard recording techniques. In particular, neither pharmacological nor voltage clamp methods are needed, as demonstrated by a recent study on the dynamics of insect auditory receptor cells (Benda et al., 2001). Third, the simplicity of the model framework allows quantitative predictions about the signal transmission properties of specific neurons arising from spike-frequency adaptation.

**7.1 Comparison with Other Adaptation Models.** Most modeling studies concerned with spike-frequency adaptation rely on a specific adaptation mechanism. Among these mechanisms, the mAHP current has been investigated intensively. Wang (1998) analyzed a conductance-based model with calcium dynamics and an mAHP current. He recognized the important difference between the time constant of the calcium removal and the effective time constant as measured from the exponential decay of the firing frequency. However, since a linear model was used, the relation between these two time constants depended on the  $f$ - $I$  curves at a given intensity ("percentage adaptation of firing frequency"). This neglects the fact that the investigated type of adaptation depends on the firing frequency and not on input intensity. In a more general investigation, Ermentrout (1998) observed the linearization of steady-state  $f$ - $I$  curves in type I neurons. He compared this result with simulations of a conductance-based model with both M-type and mAHP currents. For  $f$ - $I$  curves of the form  $f_0(I) = c\sqrt{I}$ , he derived a relation between  $\tau$  and  $\tau_{\text{eff}}$  in agreement with the more general

equation, 4.11. Adaptation in integrate-and-fire models often has been introduced by an adaptive threshold (MacGregor & Oliver, 1974; Liu & Wang, 2001). However, such thresholds may result in divisive adaptation instead of the subtractive characteristic of equation 3.1a. Quantitative differences between an adaptive threshold and an adaptation current were studied by Liu and Wang (2001) in leaky integrate-and-fire neurons.

The adaptation model introduced by Izhikevich (2000) is a specific implementation of equation 6.5 for the  $\theta$  neuron, which is up to a different scaling of variables identical to the example 6.6. It assumes a constant adaptation time constant, a steady-state adaptation strength that is proportional to the firing frequency, and a constant driving force, which is independent of the model's phase variable. This model represents the essential properties of moderate adaptation within the canonical model for type I neurons (Ermentrout, 1996). Thus, it is well suited to investigate adaptation effects for interspike intervals that are similar to or even longer than the adaptation time constant.

In the model presented here (see equation 3.1), the  $\gamma(f)$  and the  $\epsilon(f)$  terms introduce a novel frequency dependence of the averaged adaptation current and time constant, respectively.

**7.2 Model Assumptions.** The basic assumption behind model 3.1 is that the firing frequency is high compared to the inverse adaptation time constant. This is important for separating adaptation from spike generation (Cartling, 1996; Wang, 1998). Since typical adaptation time constants are larger than 50 ms, the corresponding critical firing frequency is at most 20 Hz. For peripheral neurons and regular spiking cells in the cortex (Connors & Gutnick, 1990) this is not a critical restriction. However, many central neurons fire only rarely, so that the interplay of the adaptation current with the spike generator becomes crucial. Both processes have to be analyzed in combination, for example, based on the framework of equations 6.5 and 6.7, and specific properties of the spike generator have to be taken into account.

The second main assumption is that fluctuations of the adaptation current do not strongly influence the time course of the spike dynamics. This allows one to replace the adaptation current and the adaptation time-constant and steady-state variable by averages 3.9, 3.15, and 3.16, respectively, depending only on firing frequency. The validity of this weak coupling assumption depends on the properties of the specific spike generator and is confirmed if the  $\gamma(f)$  term does not vary strongly with the adaptation state.

This assumption does not interfere with the switch from type I to type II dynamics induced by activation of M-type currents at low potentials, as pointed out by Ermentrout et al. (2001). Our description of the unadapted neuron in terms of its onset  $f$ - $I$  curve already includes this effect. In fact, since the gating variable of the M-type current obeys a linear differential equation and enters the current linearly, we can replace it by a sum of two variables. One variable covers the M-type current activated by the low po-

tentials at rest and between spikes, while the other variable is activated during spikes only. The first current is part of the spike generator and contributes to the onset  $f$ - $I$  curve and the offset of  $\tilde{\rho}(f)$  of the Crook-model, as shown in Figure 5B, and may alter a type I neuron into a type II. Only the second variable induces spike-frequency adaptation.

Following Kirchoff's law, ionic currents are additive in the membrane equation, 3.2. Therefore, adaptation caused by ionic currents is subtractive; i.e., the adapted  $f$ - $I$  curves are shifted versions of the onset  $f$ - $I$  curve. Adaptation may involve separate currents, like M-type or AHP-type currents, which obviously are additive in the membrane equation. Mechanisms acting via additional gating variables, like the slow inactivation of the sodium current, result also in an additive current, provided the other gating variables involved operate on a faster timescale. The situation is different if an adaptation process modulates the dynamics of an ionic current. For example, the level of intracellular calcium influences gene expression and could thus slowly modulate ionic currents and eventually change the shape of the  $f$ - $I$  curve (Shin, Koch, & Douglas, 1999; Stemmler & Koch, 1999).

We have shown that averaging the driving force of the adaptation current results in a constant term  $\rho$  plus higher-order terms  $\gamma(f)$  in the firing frequency  $f$ . This finding is independent of using Ohm's law, the Goldman-Hodgkin-Katz equation, or other models for membrane currents (Johnston & Wu, 1997), since we have exploited only the fact that the driving force depends on the membrane potential.

We have also assumed that the adaptation current is linearly scaled by the adaptation variable. Unlike the Hodgkin-Huxley channels, all models of the kinetics of voltage-gated adaptation currents are indeed linear (Edman et al., 1987; Fleidervish et al., 1996; Crook et al., 1998; Delord, Baraduc, Costalat, Burnod, & Guignon, 2000). However, the steady-state mAHP current may depend nonlinearly on the intracellular calcium concentration, as discussed below.

In principle, adaptation could be influenced by all biophysical processes present in the investigated cell. In many cases, however, one process is dominant. A single differential equation may then be used to capture the adaptation phenomena. Faster processes can be included into the spike generator, slower processes can be neglected, and processes with similar timescales can often be combined with this single differential equation. However, it is quite common that the timescales of the adaptation mechanisms depend on the membrane potential or calcium concentration. A single differential equation might then no longer be sufficient to describe adaptation. To our knowledge, no single current with two similar time constants exists (Hille, 1992). However, regarding adaptation due to AHP-type currents, several differential equations might indeed be involved. Another likely possibility is that several adaptation currents with similar time constants are jointly responsible for the macroscopically observed spike-frequency adaptation (Madison & Nicoll, 1984; Köhler et al., 1996; Xia et al., 1998; Stocker

et al., 1999). Their time constants could depend in different ways on the firing frequency and exclude a description in terms of a single differential equation.

**7.3 Specific Biophysical Mechanisms.** Channels carrying M-type currents are composed out of KCNQ2, KCNQ3 and KCNQ5 subunits (Wang et al., 1998; Schroeder, Hechberger, Hechenberger, Weinreich, Kubisch, & Jentsch, 2000). It is likely that different combinations of these subunits co-exist in a single neuron and that they differ in quantitative aspects of their kinetics, especially in their time constants. This could make more than one differential equation necessary for modeling the resulting spike-frequency adaptation.

The mAHP-type current is a prominent current used for modeling studies (Cartling, 1996; Ermentrout, 1998; Wang, 1998; Liu & Wang, 2001) and serves as an example for linear adaptation, governed by a single differential equation with fixed time constant. However, in contrast to M-type currents and slow recovery from inactivation, various assumptions have to be made to fit mAHP-type currents into this picture.

First, there is a possible nonlinear dependence of the mAHP current on calcium concentration. As a consequence, the adaptation current (mAHP current) would not be proportional to the adaptation state (calcium concentration). While Ermentrout (1998) and Wang (1998) do not consider this possibility, Engel, Schultens, and Schild (1999) argue for an important role of such nonlinearity. As shown by Figure 8, the shape of the steady-state  $f$ - $I$  curves of type I neurons can be linearized only if adaptation is linear; a nonlinear steady-state  $f$ - $I$  curve must result from a nonlinear adaptation and/or the  $\gamma(f)$  term. Numerous experimental data from type I neurons are in agreement with linearized steady-state  $f$ - $I$  curves (Koike, Mano, Okada, & Oshima, 1970; Gustafsson & Wigström, 1981) and suggest a linear dependence of the adaptation current on its gating variable. However, a distinct linearizing effect requires the steady-state adaptation current to be strong enough. For experimental  $f$ - $I$  curves, it is sometimes difficult to distinguish whether the steady-state  $f$ - $I$  curve is nonlinear due to weak adaptation or due to a true nonlinear adaptation (see, e.g., Madison & Nicoll, 1984; Lanthorn, Storm, & Andersen, 1984). Thus, in general, a nonlinear dependence of the adaptation current on the adaptation state cannot be ruled out.

Second, the mAHP gating variable is assumed to be fast enough so that it can be replaced by its steady-state variable. Based on mAHP channel gating data, the study of Hirschberg, Maylie, Adelman, and Marrion (1998) hints at long time constants ( $> 40$  ms) of this current at low calcium concentrations. Its dynamics cannot be neglected if this time constant exceeds the time constant of the calcium dynamics and could dominate the adaptation dynamics at low calcium levels. At higher calcium levels, calcium removal would be the prominent component. This could result in a dependence of the macroscopically observed effective adaptation time constant on the fir-

ing frequency and may even require a second differential equation for the gating variable of the mAHP current.

Third, the time constant of calcium removal could depend on firing frequency. Calcium imaging shows a decreasing time constant of the mean intracellular calcium level with increasing firing frequency (Schiller et al., 1995; Helmchen et al., 1996). This effect seems to be reproduced by detailed models of the calcium dynamics that include diffusion, pumps, and buffering (Engel et al., 1999; Schutter & Smolen, 1998), and might be important for studies on how adaptation influences the spike pattern at firing frequencies similar to the adaptation time constant.

Fourth, channels mediating the calcium influx during spikes can inactivate on a timescale of several 10 to 100 ms (Jaffe et al., 1994; Yamada, Koch, & Adams, 1998). This inactivation reduces the calcium influx per spike and thus also the strength of spike-frequency adaptation. Therefore, a further differential equation could be necessary to incorporate this process, which would act on the steady-state adaptation strength  $A_{\infty}(f)$ .

Besides the mAHP current, there exists a slow sAHP current, which induces afterhyperpolarizations and adaptation on timescales of more than 1 second (Sah & Clements, 1999; Stocker et al., 1999). There is an ongoing debate about the biophysical processes responsible (Sah & Clements, 1999). If the slow kinetics of the channels mediating the sAHP current is the dominating process, an additional differential equation for the gating of the sAHP current would be needed.

Slow recovery from inactivation has been observed for many different ionic currents. In sodium currents, it causes spike-frequency adaptation, whereas in potassium currents, it results in spike-frequency facilitation (Edman et al., 1987; Delord et al., 2000). In contrast to the M-type currents and mAHP currents, slow inactivation operates on longer timescales of about 1 second and more (French, 1989; Edman et al., 1987; Fleidervish et al., 1996; Martina & Jonas, 1997; Delord et al., 2000). From a mechanistic point of view, the only difference between spike-frequency adaptation and facilitation is that the adaptation state increases the effective input current instead of decreasing it.

Currents such as  $I_Q$  or  $I_h$  are activated by hyperpolarization (Halliwell & Adams, 1982; Maccaferri, Mangoni, Lazzari, & Di Francesco, 1993). With depolarizing inputs, these currents deactivate and contribute to spike-frequency adaptation. Their dynamics could be treated in a similar fashion as the dynamics of slow recovery from inactivation.

Sanchez-Vives, Nowak, & McCormick (2000) report a  $\text{Na}^+$ -activated  $\text{K}^+$ -current. This current induces spike-frequency adaptation on a long timescale (about 3 to 10 seconds). Since no details about the kinetics of this current are known, it remains unclear if it can be described by the adaptation model 3.1. The situation might be similar to that of the sAHP current.

Finally, electrogenic pumps have to be considered as another cause of slow adaptation (Sanchez-Vives et al., 2000). Their currents act subtractively

on the input and, in their simplest form, obey a single linear differential equation. It is therefore likely that such currents are also in agreement with the adaptation model.

In summary, many adaptation currents involved in spike generation fit into our phenomenological approach. Specific cases of adaptation due to mAHP currents and sAHP currents might be an exception. Several processes with potentially different timescales are involved in these two types of adaptation, possibly requiring more than one differential equation for a precise description of the resulting spike-frequency adaptation.

**7.4 Functional Role of Adaptation.** The shape of a neuron's  $f$ - $I$  curve is important for its signal transmission properties. Stimuli below the firing threshold  $I_{\text{th}}$  are not transmitted at all, and the slope of the  $f$ - $I$  curve limits the resolution of input modulations. In adapting neurons, the  $f$ - $I$  curve is not fixed. As we have shown, the onset  $f$ - $I$  curve is shifted dynamically by the stimulus. This shift partially compensates for the slow frequency components of the stimulus. Therefore, adaptation turns a neuron into a high-pass filter. It is the value of the effective time constant of adaptation (see equation 4.11) and not the time constant of the adaptation dynamics (see equation 3.1b), which separates slow and fast stimulus components. The latter are transmitted via the adapted  $f$ - $I$  curves. Since these are often shifted versions of the onset  $f$ - $I$  curve, the shape of the onset  $f$ - $I$  curve determines the transmission of fast components. Slow components are transmitted via the steady-state  $f$ - $I$  curve.

In this context, it should be noted that the observation that adaptation "makes the transfer function of neurons logarithmic" (Engel et al., 1999) refers to the steady-state  $f$ - $I$  curve, which is important only for the slow stimulus components. The same holds for the linearizing effect of adaptation on  $f$ - $I$  curves discussed by Ermentrout (1998).

The high-pass filter characteristics of adaptation make the response of a neuron approximately independent of the mean stimulus intensity, which is removed by shifting the  $f$ - $I$  curve. Thus, subtractive adaptation implements intensity invariance. Its fidelity depends strongly on the steady-state  $f$ - $I$  curve. For vanishing steady-state activity, the intensity invariance is achieved best. Note also that subtractive adaptation does not adapt the neuron's  $f$ - $I$  curve to higher-order statistics of the stimulus (Brenner, Bialek, & de Ruyter van Steveninck, 2000).

In order to study neural information transfer (Bialek, Rieke, de Ruyter van Steveninck, & Warland, 1991), broadband filtered white-noise stimuli with cut-off frequencies of more than 50 Hz are widely used. Since effective time constants of spike-frequency adaptation are usually larger than 10 ms, the cut-off frequency of the neuron's transfer function is well below 16 Hz. Thus, most of the stimulus power is above the cut-off frequency of adaptation. After the stimulus onset, the neuron adapts, and shortly afterward, the adaptation state stays approximately constant. Therefore, using such stim-

uli does not test adaptation. This could explain a result of French, Höger, Sekizawa, & Torkkeli (2001), who explored paired spider mechanoreceptor neurons. One of these neurons is phasic and the other phasic tonic. Surprisingly, the information transfer measured for these two types of neurons was nearly identical. However, both neurons may differ in their steady-state  $f-I$  curve while having similar onset  $f-I$  curves. For the broadband stimuli used in this experiment, only properties of the onset  $f-I$  curve contribute to the signal transmission. Therefore, the differences in the steady-state  $f-I$  curves were not tested by the stimuli, which may have resulted in the reported information rates.

Knowing the neuron's firing threshold is essential for improving stimulus reconstruction (Machens, Stemmler, Prinz, Krahe, Ronacher, & Herz, 2001). For stimuli with strong low-frequency components, the resulting varying shift of the  $f-I$  curve and its firing threshold due to adaptation would deteriorate the reconstruction. Information about the actual  $f-I$  curve as provided by the adaptation model, 3.1, could eliminate these effects.

Let us finally note that recent studies show that shunting synaptic input results in a shift of  $f-I$  curves. This corresponds formally to an adaptation current with a fixed adaptation state. However, the noisy nature of (balanced) synaptic input counteracts this shift and adds a strong divisive component on the resulting  $f-I$  curve (Chance, Abbott, & Reyes, 2002).

## Appendix

---

**A.1 List of Symbols.** The defining equations are identified in the following list:

$V$	Membrane potential
$I_X = g_X(V - E_X)$	Ionic current of type X with conductance $g_X$ and reversal potential $E_X$
$a$	Gating variable of an adaptation current
$T$	Interspike interval (ISI)
$f = 1/T$	Firing frequency
$I$	Input current
$f_0(I)$	Onset $f-I$ curve of the unadapted neuron
$f_\infty(I)$	Steady-state $f-I$ curve
$A$	Adaptation state (see equation 3.10)
$f(I; A)$	Adapted $f-I$ curve for a given adaptation state $A$
$\tilde{\rho}(f) = \rho \cdot [1 + \gamma(f)]$	Averaged driving force (see equation 3.8) of the adaptation current
$\tilde{\tau}(f) = \tau \cdot [1 + \epsilon(f)]$	Averaged time constant of the adaptation gating variable (see equation 3.15)
$\tau$	Adaptation time constant

$\kappa(f)$	Averaged steady-state adaptation variable $a_\infty(V)$ (see equation 3.16)
$A_\infty(f) = \bar{g}_A c \rho \kappa(f)$	steady-state adaptation strength (see equation 4.2)
$\tau_{\text{eff}}$	Effective adaptation time constant measured from the decay of the firing frequency evoked by a step-like stimulus
$\tau_A$	Time constant measured from the time evolution of $A$

### A.2 The Neuron's Weight Function for Small Adaptation Currents.

The superthreshold dynamics of a spike generator may be captured by a one-dimensional phase model. The phase angle  $\varphi$  describes the movement along a limit cycle, as determined by some function  $g(\varphi; I) > 0$  that depends on the phase angle and input  $I$ :

$$\frac{d\varphi}{dt} = g(\varphi; I). \quad (\text{A.1})$$

Each time the system has cycled once around the limit cycle, a spike is elicited. Equation A.1 can be expanded at some constant value  $I_0$  and transformed to a new phase variable  $\psi$  via  $d\varphi/d\psi = g(\varphi; I_0)$ ,

$$\frac{d\psi}{dt} = 1 + z(\psi; I_0)\Delta I(\psi, t), \quad (\text{A.2})$$

where  $\Delta I(\psi, t) = I(\varphi(\psi), t) - I_0$  is a small perturbation. The term

$$z(\psi; I_0) = \frac{\left. \frac{\partial g(\varphi(\psi); I)}{\partial I} \right|_{I=I_0}}{g(\varphi(\psi); I_0)} \quad (\text{A.3})$$

is the neuron's response function (Ermentrout, 1996).

Let  $T$  be the period of the perturbed phase oscillator ( $\Delta I \neq 0$ ) and  $T_0$  the period of the unperturbed phase oscillator ( $\Delta I = 0$ ). Integrating equation A.2 over one complete cycle of  $\psi$  ( $0 \leq \psi \leq T_0$ ) and expanding the integrand to first order yields

$$T \approx T_0 - \int_0^{T_0} z(\psi; I_0)\Delta I(\psi, t) d\psi, \quad (\text{A.4})$$

provided  $|z(\psi; I_0)\Delta I(\psi, t)| \ll 1$ .

In the context of averaging the adaptation current (see equation 3.6),  $I_0 = I - \langle I_A \rangle_{T,w}$  and  $T = T_0$ . We want to show that  $T$  is not changed by replacing the original  $\Delta I_A = I_A - \langle I_A \rangle_{T,w}$  by its weighted average  $\langle \Delta I_A \rangle_{T,w}$ .

This is true if the integral of the right-hand side of equation A.4 does not change if we replace  $\Delta I = \Delta I_A$  by  $\langle \Delta I_A \rangle_{T,w}$ :

$$\int_0^T z(\psi; I_0) \Delta I_A(\psi) d\psi \stackrel{!}{=} \int_0^T z(\psi; I_0) \langle \Delta I_A(\psi) \rangle_{T,w} d\psi. \quad (\text{A.5})$$

Since the average  $\langle \Delta I_A \rangle_{T,w}$  is constant during one period  $T$ , we obtain

$$\langle \Delta I_A \rangle_{T,w} = \frac{\int_0^T z(\psi; I_0) \Delta I_A(\psi) d\psi}{\int_0^T z(\psi; I_0) d\psi} =: \int_0^T \tilde{z}(\psi; I_0) \Delta I_A(\psi) d\psi. \quad (\text{A.6})$$

This shows that replacing  $\Delta I_A$  by the weighted average  $\langle \Delta I_A \rangle_{T,w}$  has no effect on  $T$  if the weight  $w$  is given by the neuron's normalized response function  $\tilde{z}$ . The weight  $w(t)$  in equation 3.6 is then given by  $\tilde{z}(\psi(t)) \cdot d\psi(t)/dt$ .

Note that because of the assumption  $|z(\psi; I_0) \Delta I_A(\psi, t)| \ll 1$ , this finding is true in the limit for small adaptation currents only. Numerical simulations of  $z \cdot \Delta I$  for the models used in this article result in values larger than one. For such strong adaptation currents, the weight  $w$  in equation 3.6 does not equal  $\tilde{z}$ , since  $\tilde{z}$  applies to small perturbations only. However, the appropriate weight  $w$  might still reflect the main qualitative properties of the neuron's response function.

### A.3 Specification of the Conductance-Based Models

*A.3.1 Modified Traub-Miles Model.* The modified Traub-Miles model was introduced by Ermentrout (1998). It is a single compartment model with one sodium, potassium, and calcium current. We added either an M-type current or an mAHP current to induce spike-frequency adaptation:

$$C \frac{dV}{dt} = -I_{\text{Na}} - I_{\text{K}} - I_{\text{Ca}} - I_{\text{L}} - I_{\text{M}} - I_{\text{mAHP}} + I$$

$$C = 1 \mu\text{F}/\text{cm}^2.$$

Sodium current:  $I_{\text{Na}} = \bar{g}_{\text{Na}} m^3 h (V - E_{\text{Na}})$ ,  $\bar{g}_{\text{Na}} = 100 \text{ mS}/\text{cm}^2$ ,  $E_{\text{Na}} = +50 \text{ mV}$ ,  $dm/dt = \alpha_m(V)(1-m) - \beta_m(V)m$ ,  $\alpha_m(V) = 0.32(V+54)/(1 - \exp(-(V+54)/4))$ ,  $\beta_m(V) = 0.28(V+27)/(\exp((V+27)/5)-1)$ ,  $dh/dt = \alpha_h(V)(1-h) - \beta_h(V)h$ ,  $\alpha_h(V) = 0.128 \exp(-(V+50)/18)$ ,  $\beta_h(V) = 4/(1 + \exp(-(V+27)/5))$ .

Potassium delayed-rectifier current:  $I_{\text{K}} = \bar{g}_{\text{K}} n^4 (V - E_{\text{K}})$ ,  $\bar{g}_{\text{K}} = 80 \text{ mS}/\text{cm}^2$ ,  $E_{\text{K}} = -100 \text{ mV}$ ,  $dn/dt = \alpha_n(V)(1-n) - \beta_n(V)n$ ,  $\alpha_n(V) = 0.032(V+52)/(1 - \exp(-(V+52)/5))$ ,  $\beta_n(V) = 0.5 \exp(-(V+57)/40)$ .

Calcium current:  $I_{\text{Ca}} = \bar{g}_{\text{Ca}} s_{\infty}(V)(V - E_{\text{Ca}})$ ,  $\bar{g}_{\text{Ca}} = 5 \text{ mS}/\text{cm}^2$ ,  $E_{\text{Ca}} = 120 \text{ mV}$ ,  $s_{\infty}(V) = 1/(1 + \exp(-(V+25)/5))$ .

Leakage current:  $I_{\text{L}} = \bar{g}_{\text{L}}(V - E_{\text{L}})$ ,  $\bar{g}_{\text{L}} = 0.1 \text{ mS}/\text{cm}^2$ ,  $E_{\text{L}} = -67 \text{ mV}$ .

M-type current:  $I_M = \bar{g}_M w(V - E_M)$ ,  $\bar{g}_M = 8 \text{ mS/cm}^2$ ,  $E_M = -100 \text{ mV}$ ,  $\tau_w(V) \frac{dw}{dt} = w_\infty(V) - w$ ,  $\tau_w(V) = 100 \text{ ms}$ ,  $w_\infty(V) = 1/(1 + \exp(-(V + 20)/5))$ .

mAHP-current and calcium dynamics:  $I_{\text{mAHP}} = \bar{g}_{\text{mAHP}} q(V - E_{\text{mAHP}})$ ,  $\bar{g}_{\text{mAHP}} = 4 \text{ mS/cm}^2$ ,  $E_{\text{mAHP}} = -100 \text{ mV}$ ,  $q = [\text{Ca}]/(30 + [\text{Ca}])$ ,  $d[\text{Ca}]/dt = -0.002I_{\text{Ca}} - 0.0125[\text{Ca}]$ .

*A.3.2 Crook Model.* We used the model of Crook et al. (1998) with only the M-type current as an additional example of an adapting neuron. It is a two-compartment model. One compartment corresponds to the soma and is modeled by the membrane equation for the potential  $V_s$  of the soma. It contains all the voltage-dependent currents for the generation of spikes and possible adaptation currents. The other compartment captures the whole dendritic tree and is described by a linear membrane equation. The potential of the second compartment is denoted by  $V_d$ . Both compartments are coupled by the coupling current  $I_C$ . Note that the input current  $I$  is injected into the soma. Therefore, the adaptation currents are still additive to the input current. The resting potential of the Crook model is at  $-77 \text{ mV}$ :

$$C \frac{dV_s}{dt} = -I_{\text{Na}} - I_{\text{K}} - I_{\text{Ca}} - I_{\text{LS}} - I_{\text{M}} - I_C/P + I/P$$

$$C \frac{dV_d}{dt} = -I_{\text{LD}} + I_C/(1 - P)$$

$$C = 0.8 \text{ } \mu\text{F/cm}^2, P = 0.05.$$

Sodium current:  $I_{\text{Na}} = \bar{g}_{\text{Na}} m^2 h(V_s - E_{\text{Na}})$ ,  $\bar{g}_{\text{Na}} = 221 \text{ mS/cm}^2$ ,  $E_{\text{Na}} = +55 \text{ mV}$ ,  $dm/dt = \alpha_m(V)(1 - m) - \beta_m(V)m$ ,  $\alpha_m(V) = 0.32(-47.1 - V_s)/(\exp(0.25(-47.1 - V_s)) - 1)$ ,  $\beta_m(V) = 0.28(V_s + 20.1)/(\exp((V_s + 20.1)/5) - 1)$ ,  $dh/dt = \alpha_h(V)(1 - h) - \beta_h(V)h$ ,  $\alpha_h(V) = 0.128 \exp((-43 - V_s)/18)$ ,  $\beta_h(V) = 4/(\exp((-20 - V_s)/5) + 1)$ .

Potassium delayed-rectifier current:  $I_{\text{K}} = \bar{g}_{\text{K}} n(V_s - E_{\text{K}})$ ,  $\bar{g}_{\text{K}} = 47 \text{ mS/cm}^2$ ,  $E_{\text{K}} = -90 \text{ mV}$ ,  $dn/dt = \alpha_n(V)(1 - n) - \beta_n(V)n$ ,  $\alpha_n(V) = 0.59(-25.1 - V_s)/(\exp((-25.1 - V_s)/5) - 1)$ ,  $\beta_n(V) = 0.925 \exp(0.925 - 0.025(V_s + 77))$ .

Calcium current:  $I_{\text{Ca}} = \bar{g}_{\text{Ca}} s^2 r(V_s - E_{\text{Ca}})$ ,  $\bar{g}_{\text{Ca}} = 8.5 \text{ mS/cm}^2$ ,  $E_{\text{Ca}} = +120 \text{ mV}$ ,  $ds/dt = \alpha_s(V)(1 - s) - \beta_s(V)s$ ,  $\alpha_s(V) = 0.912/(\exp(-0.072(V_s - 5)) + 1)$ ,  $\beta_s(V) = 0.0114(V_s + 8.9)/(\exp((V_s + 8.9)/5) - 1)$ ,  $\tau_r(V) dr/dt = r_\infty(V) - r$ ,  $r_\infty(V) = \min(\exp(-(V_s + 60)/20), 1)$ ,  $\tau_r(V) = 200 \text{ ms}$ .

Soma leakage-current:  $I_{\text{LS}} = \bar{g}_{\text{LS}}(V_s - E_{\text{LS}})$ ,  $\bar{g}_{\text{LS}} = 2 \text{ mS/cm}^2$ ,  $E_{\text{LS}} = -70 \text{ mV}$ .

M-type current:  $I_{\text{M}} = \bar{g}_{\text{M}} w(V_s - E_{\text{K}})$ ,  $\bar{g}_{\text{M}} = 10 \text{ mS/cm}^2$ ,  $E_{\text{K}} = -90 \text{ mV}$ ,  $\tau_w(V) \frac{dw}{dt} = w_\infty(V) - w$ ,  $w_\infty(V) = 1/(\exp(-(V_s + 35)/10) + 1)$ ,

$$\tau_w(V) = 92 \exp(-(V_s + 35)/20)/(1 + 0.3 \exp(-(V_s + 35)/10)).$$

$$\text{Dendrite leakage-current: } I_{LD} = \bar{g}_{LD}(V_d - E_{LD}), \bar{g}_{LD} = 0.05 \text{ mS/cm}^2, \\ E_{LD} = -70 \text{ mV}.$$

$$\text{Coupling current: } I_C = \bar{g}_C(V_s - V_d), [\bar{g}_C = 1.1 \text{ mS/cm}^2].$$

### Acknowledgments

---

We thank Matthias Bethge, Paola Pedarzani, and Lorenzo Cingolani for important discussions and references. We are grateful to Hartmut Schütze, Matthias Hennig, Astrid Franz, Bernhard Ronacher, Tim Gollisch, Christian Machens, Raphael Ritz, Laurenz Wiskott, and Martin Stemmler who contributed to this work with helpful suggestions and experimental evidence. This work was supported by the DFG through GK 120 and Innovationskolleg Theoretische Biologie.

### References

---

- Benda, J., Bethge, M., Hennig, M., Pawelzik, K., & Herz, A. V. M. (2001). Spike-frequency adaptation: Phenomenological model and experimental tests. *Neurocomput.*, 38–40, 105–110.
- Bialek, W., Rieke, F., de Ruyter van Steveninck, R. R., & Warland, D. (1991). Reading a neural code. *Science*, 252, 1854–1857.
- Brenner, N., Bialek, W., & de Ruyter van Steveninck, R. (2000). Adaptive rescaling maximizes information transfer. *Neuron*, 26, 695–702.
- Brown, D. A., & Adams, P. R. (1980). Muscarinic suppression of a novel voltage-sensitive  $K^+$  current in a vertebrate neuron. *Nature*, 183, 673–676.
- Brown, D. A., & Griffith, W. H. (1983). Calcium-activated outward current in voltage-clamped hippocampal neurones of the guinea-pig. *J. Physiol.*, 337, 287–301.
- Cartling, B. (1996). A low-dimensional, time resolved and adapting model neuron. *Int. J. Neural Syst.*, 7, 237–246.
- Chance, F. S., Abbott, L. F., & Reyes, A. D. (2002). Gain modulation from background synaptic input. *Neuron*, 35, 773–782.
- Connors, B. W., & Gutnick, M. J. (1990). Intrinsic firing patterns of diverse neocortical neurons. *Trends Neurosci.*, 13, 99–104.
- Crook, S. M., Ermentrout, G. B., & Bower, J. M. (1998). Spike frequency adaptation affects the synchronization properties of networks of cortical oscillators. *Neural Comput.*, 10, 837–854.
- Delord, B., Baraduc, P., Costalat, R., Burnod, Y., & Guigon, E. (2000). A model study of cellular short-term memory produced by slowly inactivating potassium conductances. *J. Comput. Neurosci.*, 8, 251–273.
- Edman, Å, Gestrelus, S., & Grampp, W. (1987). Analysis of gated membrane currents and mechanisms of firing control in the rapidly adapting lobster stretch receptor neurone. *J. Physiol.*, 384, 649–669.

- Engel, J., Schultens, H. A., & Schild, D. (1999). Small conductance potassium channels cause an activity-dependent spike frequency adaptation and make the transfer function of neurons logarithmic. *Biophys. J.*, *76*, 1310–1319.
- Ermentrout, B. (1996). Type I membranes, phase resetting curves, and synchrony. *Neural Comput.*, *8*, 979–1001.
- Ermentrout, B. (1998). Linearization of  $f$ - $I$  curves by adaptation. *Neural Comput.*, *10*, 1721–1729.
- Ermentrout, B., Pascal, M., & Gutkin, B. (2001). The effects of spike frequency adaptation and negative feedback on the synchronization of neural oscillators. *Neural Comput.*, *13*, 1285–1310.
- Fleiderovich, I. A., Friedman, A., & Gutnick, M. J. (1996). Slow inactivation of  $\text{Na}^+$  current and slow cumulative spike adaptation in mouse and guinea-pig neocortical neurones in slices. *J. Physiol.*, *493.1*, 83–97.
- French, A. S. (1989). Two components of rapid sensory adaptation in a cockroach mechanoreceptor neuron. *J. Neurophys.*, *62*, 768–777.
- French, A. S., Höger, U., Sekizawa, S.-I., & Torkkeli, P. H. (2001). Frequency response functions and information capacities of paired spider mechanoreceptor neurons. *Biol. Cybern.*, *85*, 293–300.
- Gustafsson, B., & Wigström, H. (1981). Shape of frequency-current curves in CA1 pyramidal cells in the hippocampus. *Brain Res.*, *223*, 417–421.
- Halliwel, J. V., & Adams, P. R. (1982). Voltage-clamp analysis of muscarinic excitation in hippocampal neurons. *Brain Res.*, *250*, 71–92.
- Hansel, D., Mato, G., & Meunier, C. (1995). Synchrony in excitatory neural networks. *Neural Comput.*, *7*, 307–337.
- Helmchen, F., Imoto, K., & Sakmann, B. (1996).  $\text{Ca}^{2+}$  buffering and action potential-evoked  $\text{Ca}^{2+}$  signaling in dendrites of pyramidal neurons. *Biophys. J.*, *70*, 1069–1081.
- Hille, B. (1992). *Ionic membranes of excitable membranes* (2nd ed.). Sunderland, Sinauer Associates.
- Hirschberg, B., Maylie, J., Adelman, J. P., & Marrion, N. V. (1998). Gating of recombinant small-conductance  $\text{Ca}$ -activated  $\text{K}^+$  channels by calcium. *J. Gen. Physiol.*, *111*, 565–581.
- Hodgkin, A. L. (1948). The local electric changes associated with repetitive action in a non-medullated axon. *J. Physiol.*, *107*, 165–181.
- Hodgkin, A. L., & Huxley, A. F. (1952). A quantitative description of membrane current and its application to conduction and excitation in nerve. *J. Physiol.*, *117*, 500–544.
- Hoppensteadt, F. C., & Izhikevich, E. M. (1997). *Weakly connected neural networks*. New York: Springer-Verlag.
- Izhikevich, E. M. (2000). Neural excitability, spiking, and bursting. *Int. J. Bif. Chaos*, *10*, 1171–1266.
- Jaffe, D. B., Ross, W. N., Lisman, J. E., Lasser-Ross, N., Miyakawa, H., & Johnston, D. (1994). A model for dendritic  $\text{Ca}^{2+}$  accumulation in hippocampal pyramidal neurons based on fluorescence imaging measurements. *J. Neurophys.*, *71*, 1065–1077.
- Johnston, D., & Wu, S. M.-S. (1997). *Foundations of cellular neurophysiology*. Cambridge, MA: MIT Press.

- Köhler, M., Hirschberg, B., Bond, C. T., Kinzie, J. M., Marrion, N. V., Maylie, J., & Adelman, J. P. (1996). Small-conductance, calcium activated potassium channels from mammalian brain. *Science*, *273*, 1709–1714.
- Koike, H., Mano, N., Okada, Y., & Oshima, T. (1970). Repetitive impulses generated in fast and slow pyramidal tract cells by intracellularly applied current steps. *Exp. Brain Res.*, *11*, 263–281.
- Lanthorn, T., Storm, J., & Andersen, P. (1984). Current-to-frequency transduction in CA1 hippocampal pyramidal cells: Slow prepotentials dominate the primary range firing. *Exp. Brain Res.*, *53*, 431–443.
- Liu, Y.-H., & Wang, X.-J. (2001). Spike-frequency adaptation of a generalized leaky integrate-and-fire model neuron. *J. Comput. Neurosci.*, *10*, 25–45.
- Maccaferri, G., Mangoni, M., Lazzari, A., & DiFrancesco, D. (1993). Properties of the hyperpolarization-activated current in rat hippocampal CA1 pyramidal cells. *J. Neurophys.*, *69*, 2129–2136.
- MacGregor, R. J., & Oliver, R. M. (1974). A model for repetitive firing in neurons. *Kybernetik*, *16*, 53–64.
- Machens, C. K., Stemmler, M. B., Prinz, P., Krahe, R., Ronacher, B., & Herz, A. V. (2001). Representation of acoustic communication signals by insect auditory receptor neurons. *J. Neurosci.*, *21*, 3215–3227.
- Madison, D. V., & Nicoll, R. A. (1984). Control of the repetitive discharge of rat CA1 pyramidal neurones in vitro. *J. Physiol.*, *354*, 319–331.
- Martina, M., & Jonas, P. (1997). Functional differences in Na<sup>+</sup> channel gating between fast-spiking interneurons and principal neurons of rat hippocampus. *J. Physiol.*, *505.3*, 593–603.
- Reyes, A. D., & Fetz, E. E. (1993). Two modes of interspike interval shortening by brief transient depolarizations in cat neocortical neurones. *J. Neurophys.*, *69*, 1661–1672.
- Sah, P., & Clements, J. D. (1991). Photolytic manipulation of [Ca<sub>2+</sub>]<sub>i</sub> reveals slow kinetics of potassium channels underlying the afterhyperpolarization in hippocampal pyramidal neurons. *J. Neurosci.*, *19*, 3657–3664.
- Sanchez-Vives, M. V., Nowak, L. G., & McCormick, D. A. (2000). Cellular mechanisms of long-lasting adaptation in visual cortical neurons in vitro. *J. Neurosci.*, *20*, 4286–4299.
- Sandler, V. M. & Barbara, J.-G. (1999). Calcium-induced calcium release contributes to action potential-evoked calcium transients in hippocampal CA1 pyramidal neurons. *J. Neurosci.*, *19*, 4325–4336.
- Schiller, J., Helmchen, F., & Sakmann, B. (1995). Spatial profile of dendritic calcium transients evoked by action potentials in rat neocortical pyramidal neurons. *J. Physiol.*, *487.3*, 583–600.
- Schroeder, B. C., Hechenberger, M., Weinreich, F., Kubisch, C., & Jentsch, T. J. (2000). KCNQ5, a novel potassium channel broadly expressed in brain, mediates M-type currents. *J. Biol. Chem.*, *275*, 24089–24095.
- Schutter, E. D. & Smolen, P. (1998). Calcium dynamics in large neuronal models. In C. Koch & I. Segev (Eds.), *Methods in neural modeling* (pp. 211–250). Cambridge, MA: MIT Press.
- Schwandt, P. E. (1973). Membrane-potential trajectories underlying motoneuron rhythmic firing at high rates. *J. Neurophys.*, *36*, 434–449.

- Shin, J., Koch, C., & Douglas, R. (1999). Adaptive neural coding dependent on the time-varying statistics of the somatic input current. *Neural Comput.*, *11*, 1893–1913.
- Stemmler, M., & Koch, C. (1999). How voltage-dependent conductances can adapt to maximize the information encoded by neuronal firing rate. *Nat. Neurosci.*, *2*, 521–527.
- Stocker, M., Krause, M., & Pedarzani, P. (1999). An apamin-sensitive  $\text{Ca}^{2+}$ -activated  $\text{K}^+$  current in hippocampal pyramidal neurons. *Proc. Natl. Acad. Sci. USA*, *96*, 4662–4667.
- Traub, R. D., Wong, R. K. S., Miles, R., & Michelson, H. (1991). A model of a CA3 hippocampal pyramidal neuron incorporating voltage-clamp data on intrinsic conductances. *J. Neurophys.*, *66*, 635–650.
- Wang, H.-S., Pan, Z., Shi, W., Brown, B. S., Wymore, R. S., Cohen, I. S., Dixon, J. E., & McKinnon, D. (1998). KCNQ2 and KCNQ3 potassium channel subunits: Molecular correlates of the M-channel. *Science*, *282*, 1890–1893.
- Wang, X.-J. (1998). Calcium coding and adaptive temporal computation in cortical pyramidal neurons. *J. Neurophys.*, *79*, 1549–1566.
- Xia, X.-M., Fakler, B., Rivard, A., Wayman, G., Johnson-Pais, T., Keen, J., Ishii, T., Hirschberg, B., Bond, C., Lutsenko, S., Maylie, J., & Adelman, J. (1998). Mechanisms of calcium gating in small-conductance calcium-activated potassium channels. *Nature*, *395*, 503–507.
- Yamada, W. M., Koch, C., & Adams, P. R. (1998). Multiple channels and calcium dynamics. In C. Koch & I. Segev (Eds.), *Methods in neural modeling* (pp. 137–170). Cambridge, MA: MIT Press.

**This article has been cited by:**

1. Javier del Valle, Pavel Salev, Yoav Kalcheim, Ivan K. Schuller. 2020. A caloritronics-based Mott neuristor. *Scientific Reports* **10**:1. . [[Crossref](#)]
2. Johannes Partzsch, Christian Mayr, Massimiliano Giulioni, Marko Noack, Stefan Hänzsche, Stefan Scholze, Sebastian Höppner, Paolo Del Giudice, Rene Schüffny. 2020. Mean Field Approach for Configuring Population Dynamics on a Biohybrid Neuromorphic System. *Journal of Signal Processing Systems* **9**. . [[Crossref](#)]
3. Sourav Dutta, Clemens Schafer, Jorge Gomez, Kai Ni, Siddharth Joshi, Suman Datta. 2020. Supervised Learning in All FeFET-Based Spiking Neural Network: Opportunities and Challenges. *Frontiers in Neuroscience* **14**. . [[Crossref](#)]
4. Owen Y. Chao, Ezequiel Marron Fernandez de Velasco, Salil Saurav Pathak, Swati Maitra, Hao Zhang, Lisa Duvick, Kevin Wickman, Harry T. Orr, Hirokazu Hirai, Yi-Mei Yang. 2020. Targeting inhibitory cerebellar circuitry to alleviate behavioral deficits in a mouse model for studying idiopathic autism. *Neuropsychopharmacology* **45**:7, 1159-1170. [[Crossref](#)]
5. Yunjiao Wang, Zachary P. Kilpatrick, Krešimir Josić. 2020. A hierarchical model of perceptual multistability involving interocular grouping. *Journal of Computational Neuroscience* **14**. . [[Crossref](#)]
6. Chittotosh Ganguly, Saswat Chakrabarti. 2020. A Discrete Time Framework for Spike Transfer Process in a Cortical Neuron With Asynchronous EPSP, IPSP, and Variable Threshold. *IEEE Transactions on Neural Systems and Rehabilitation Engineering* **28**:4, 772-781. [[Crossref](#)]
7. Hui Zhang, Jing Yao, Lianchun Yu, Yiqi Zhang. 2020. The noise cancelation effects caused by spike-frequency adaptation in single neurons. *Nonlinear Dynamics* **100**:2, 1825-1835. [[Crossref](#)]
8. Paul Pfeiffer, Alexei V Egorov, Franziska Lorenz, Jan-Hendrik Schleimer, Andreas Draguhn, Susanne Schreiber. 2020. Clusters of cooperative ion channels enable a membrane-potential-based mechanism for short-term memory. *eLife* **9**. . [[Crossref](#)]
9. Mauricio Girardi-Schappo, Ludmila Brochini, Ariadne A. Costa, Tawan T. A. Carvalho, Osame Kinouchi. 2020. Synaptic balance due to homeostatically self-organized quasicritical dynamics. *Physical Review Research* **2**:1. . [[Crossref](#)]
10. Taehyung Kim, Kyungchul Park, Taejin Jang, Myung-Hyun Baek, Young Suh Song, Byung-Gook Park. 2020. Input-modulating adaptive neuron circuit employing asymmetric floating-gate MOSFET with two independent control gates. *Solid-State Electronics* **163**, 107667. [[Crossref](#)]
11. Saray Soldado-Magraner, Federico Brandalise, Suraj Honnuraiah, Michael Pfeiffer, Marie Moulinier, Urs Gerber, Rodney Douglas. 2020. Conditioning by subthreshold synaptic input changes the intrinsic firing pattern of CA3 hippocampal neurons. *Journal of Neurophysiology* **123**:1, 90-106. [[Crossref](#)]
12. Steffen Krüppel, Christian Tetzlaff. 2020. The self-organized learning of noisy environmental stimuli requires distinct phases of plasticity. *Network Neuroscience* **4**:1, 174-199. [[Abstract](#)] [[Full Text](#)] [[PDF](#)] [[PDF Plus](#)] [[Supplemental Material](#)]
13. Jan Grewe. Peripheral High-Frequency Electrosensory Systems . [[Crossref](#)]
14. Joachim Mogdans. Physiology of the Peripheral Lateral Line System . [[Crossref](#)]
15. Alexander Vahl, Jürgen Carstensen, Sören Kaps, Oleg Lupan, Thomas Strunskus, Rainer Adelung, Franz Faupel. 2019. Concept and modelling of memsensors as two terminal devices with enhanced capabilities in neuromorphic engineering. *Scientific Reports* **9**:1. . [[Crossref](#)]
16. Sonja Meiser, Go Ashida, Jutta Kretzberg. 2019. Non-synaptic Plasticity in Leech Touch Cells. *Frontiers in Physiology* **10**. . [[Crossref](#)]
17. Urit Gordon, Shimon Marom, Naama Brenner. 2019. Visual detection of time-varying signals: Opposing biases and their timescales. *PLOS ONE* **14**:11, e0224256. [[Crossref](#)]
18. Lubomir Kostal, Ryota Kobayashi. 2019. Critical size of neural population for reliable information transmission. *Physical Review E* **100**:5. . [[Crossref](#)]
19. Maurizio Mattia, Matteo Biggio, Andrea Galluzzi, Marco Storace. 2019. Dimensional reduction in networks of non-Markovian spiking neurons: Equivalence of synaptic filtering and heterogeneous propagation delays. *PLOS Computational Biology* **15**:10, e1007404. [[Crossref](#)]
20. Andreas Stumpner, Paule Chloé Lefebvre, Marvin Seifert, Tim Daniel Ostrowski. 2019. Temporal processing properties of auditory DUM neurons in a bush-cricket. *Journal of Comparative Physiology A* **205**:5, 717-733. [[Crossref](#)]
21. Alison I Weber, Adrienne L Fairhall. 2019. The role of adaptation in neural coding. *Current Opinion in Neurobiology* **58**, 135-140. [[Crossref](#)]
22. Sebastian Vellmer, Benjamin Lindner. 2019. Theory of spike-train power spectra for multidimensional integrate-and-fire neurons. *Physical Review Research* **1**:2. . [[Crossref](#)]

23. Sukbin Lim. 2019. Mechanisms underlying sharpening of visual response dynamics with familiarity. *eLife* **8**. . [[Crossref](#)]
24. Mohammed F. Tolba, Abdulaziz H. Elsafty, Mina Armanyos, Lobna A. Said, Ahmed H. Madian, Ahmed G. Radwan. 2019. Synchronization and FPGA realization of fractional-order Izhikevich neuron model. *Microelectronics Journal* **89**, 56-69. [[Crossref](#)]
25. Samuel P. Muscinelli, Wulfram Gerstner, Tilo Schwalger. 2019. How single neuron properties shape chaotic dynamics and signal transmission in random neural networks. *PLOS Computational Biology* **15**:6, e1007122. [[Crossref](#)]
26. Chittotosh Ganguly, Saswat Chakrabarti. 2019. A leaky integrate and fire model for spike generation in a neuron with variable threshold and multiple-input-single-output configuration. *Transactions on Emerging Telecommunications Technologies* **30**:7, e3561. [[Crossref](#)]
27. Michael Jan Fauth, Mark CW van Rossum. 2019. Self-organized reactivation maintains and reinforces memories despite synaptic turnover. *eLife* **8**. . [[Crossref](#)]
28. Malte Kähne, Sten Rüdiger, Alexandre Hiroaki Kihara, Benjamin Lindner. 2019. Gap junctions set the speed and nucleation rate of stage I retinal waves. *PLOS Computational Biology* **15**:4, e1006355. [[Crossref](#)]
29. Manuel Beiran, Srdjan Ostojic. 2019. Contrasting the effects of adaptation and synaptic filtering on the timescales of dynamics in recurrent networks. *PLOS Computational Biology* **15**:3, e1006893. [[Crossref](#)]
30. Thomas D. Helton, Meilan Zhao, Shannon Farris, Serena M. Dudek. 2019. Diversity of dendritic morphology and entorhinal cortex synaptic effectiveness in mouse CA2 pyramidal neurons. *Hippocampus* **29**:2, 78-92. [[Crossref](#)]
31. Victor J. Barranca, Han Huang, Sida Li. 2019. The impact of spike-frequency adaptation on balanced network dynamics. *Cognitive Neurodynamics* **13**:1, 105-120. [[Crossref](#)]
32. Diana E Mitchell, Annie Kwan, Jerome Carriot, Maurice J Chacron, Kathleen E Cullen. 2018. Neuronal variability and tuning are balanced to optimize naturalistic self-motion coding in primate vestibular pathways. *eLife* **7**. . [[Crossref](#)]
33. L. Guarina, C. Calorio, D. Gavello, E. Moreva, P. Traina, A. Battiato, S. Ditalia Tchernij, J. Forneris, M. Gai, F. Picollo, P. Olivero, M. Genovese, E. Carbone, A. Marcantoni, V. Carabelli. 2018. Nanodiamonds-induced effects on neuronal firing of mouse hippocampal microcircuits. *Scientific Reports* **8**:1. . [[Crossref](#)]
34. Chengjie G Huang, Michael G Metzzen, Maurice J Chacron. 2018. Feedback optimizes neural coding and perception of natural stimuli. *eLife* **7**. . [[Crossref](#)]
35. Timothy George Bayley, Berthold Hedwig. 2018. Dendritic Ca<sup>2+</sup> dynamics and multimodal processing in a cricket antennal interneuron. *Journal of Neurophysiology* **120**:3, 910-919. [[Crossref](#)]
36. T. Kim, M.H. Oh, M.W. Kwon, B.-G. Park. 2018. Integrate-and-fire spiking neuron circuit exhibiting spike-triggered adaptation through input current modulation with back gate effect. *Electronics Letters* **54**:17, 1022-1024. [[Crossref](#)]
37. Wilten Nicola, Peter John Hellyer, Sue Ann Campbell, Claudia Clopath. 2018. Chaos in homeostatically regulated neural systems. *Chaos: An Interdisciplinary Journal of Nonlinear Science* **28**:8, 083104. [[Crossref](#)]
38. Alex D. Bird, Magnus J. E. Richardson. 2018. Transmission of temporally correlated spike trains through synapses with short-term depression. *PLOS Computational Biology* **14**:6, e1006232. [[Crossref](#)]
39. Christian Klos, Daniel Miner, Jochen Triesch. 2018. Bridging structure and function: A model of sequence learning and prediction in primary visual cortex. *PLOS Computational Biology* **14**:6, e1006187. [[Crossref](#)]
40. Luozheng Li, Yuanyuan Mi, Wenhao Zhang, Da-Hui Wang, Si Wu. 2018. Dynamic Information Encoding With Dynamic Synapses in Neural Adaptation. *Frontiers in Computational Neuroscience* **12**. . [[Crossref](#)]
41. Siva Venkadesh, Alexander O. Komendantov, Stanislav Listopad, Eric O. Scott, Kenneth De Jong, Jeffrey L. Krichmar, Giorgio A. Ascoli. 2018. Evolving Simple Models of Diverse Intrinsic Dynamics in Hippocampal Neuron Types. *Frontiers in Neuroinformatics* **12**. . [[Crossref](#)]
42. Wondimu W. Teka, Ranjit Kumar Upadhyay, Argha Mondal. 2018. Spiking and bursting patterns of fractional-order Izhikevich model. *Communications in Nonlinear Science and Numerical Simulation* **56**, 161-176. [[Crossref](#)]
43. Ken Takiyama. 2017. Influence of neural adaptation on dynamics and equilibrium state of neural activities in a ring neural network. *Journal of Physics A: Mathematical and Theoretical* **50**:49, 495601. [[Crossref](#)]
44. Pradeep Kuravi, Rufin Vogels. 2017. Effect of adapter duration on repetition suppression in inferior temporal cortex. *Scientific Reports* **7**:1. . [[Crossref](#)]
45. Arthur S. Sherman, Joon Ha. 2017. How Adaptation Makes Low Firing Rates Robust. *The Journal of Mathematical Neuroscience* **7**:1. . [[Crossref](#)]
46. Ran Rubin, L. F. Abbott, Haim Sompolinsky. 2017. Balanced excitation and inhibition are required for high-capacity, noise-robust neuronal selectivity. *Proceedings of the National Academy of Sciences* **114**:44, E9366-E9375. [[Crossref](#)]

47. Wondimu W. Teka, Ranjit Kumar Upadhyay, Argha Mondal. 2017. Fractional-order leaky integrate-and-fire model with long-term memory and power law dynamics. *Neural Networks* **93**, 110-125. [[Crossref](#)]
48. Ariadne Costa, Ludmila Brochini, Osame Kinouchi. 2017. Self-Organized Supercriticality and Oscillations in Networks of Stochastic Spiking Neurons. *Entropy* **19**:8, 399. [[Crossref](#)]
49. Chengjie G. Huang, Maurice J. Chacron. 2017. SK channel subtypes enable parallel optimized coding of behaviorally relevant stimulus attributes: A review. *Channels* **11**:4, 281-304. [[Crossref](#)]
50. Joachim Mogdans, Christina Müller, Maren Frings, Ferdinand Raap. 2017. Adaptive responses of peripheral lateral line nerve fibres to sinusoidal wave stimuli. *Journal of Comparative Physiology A* **203**:5, 329-342. [[Crossref](#)]
51. Wilhelm Braun, Rüdiger Thul, André Longtin. 2017. Evolution of moments and correlations in nonrenewal escape-time processes. *Physical Review E* **95**:5. . [[Crossref](#)]
52. Christoph Fretter, Annick Lesne, Claus C. Hilgetag, Marc-Thorsten Hütt. 2017. Topological determinants of self-sustained activity in a simple model of excitable dynamics on graphs. *Scientific Reports* **7**:1. . [[Crossref](#)]
53. William C. Buchta, Stephen V. Mahler, Benjamin Harlan, Gary S. Aston-Jones, Arthur C. Riegel. 2017. Dopamine terminals from the ventral tegmental area gate intrinsic inhibition in the prefrontal cortex. *Physiological Reports* **5**:6, e13198. [[Crossref](#)]
54. Felipe Gerhard, Moritz Deger, Wilson Truccolo. 2017. On the stability and dynamics of stochastic spiking neuron models: Nonlinear Hawkes process and point process GLMs. *PLoS Computational Biology* **13**:2, e1005390. [[Crossref](#)]
55. Bonan Shan, Jiang Wang, Lvxia Zhang, Bin Deng, Xile Wei. 2017. Fitting of adaptive neuron model to electrophysiological recordings using particle swarm optimization algorithm. *International Journal of Modern Physics B* **31**:05, 1750023. [[Crossref](#)]
56. Jannis Schuecker, Maximilian Schmidt, Sacha J. van Albada, Markus Diesmann, Moritz Helias. 2017. Fundamental Activity Constraints Lead to Specific Interpretations of the Connectome. *PLoS Computational Biology* **13**:2, e1005179. [[Crossref](#)]
57. T.G. Correale, L.H.A. Monteiro. 2016. On the dynamics of axonal membrane: Ion channel as the basic unit of a deterministic model. *Applied Mathematics and Computation* **291**, 292-302. [[Crossref](#)]
58. Ludmila Brochini, Ariadne de Andrade Costa, Miguel Abadi, Antônio C. Roque, Jorge Stolfi, Osame Kinouchi. 2016. Phase transitions and self-organized criticality in networks of stochastic spiking neurons. *Scientific Reports* **6**:1. . [[Crossref](#)]
59. Maxim Komarov, Maxim Bazhenov. 2016. Linking dynamics of the inhibitory network to the input structure. *Journal of Computational Neuroscience* **41**:3, 367-391. [[Crossref](#)]
60. Guo-Sheng Yi, Jiang Wang, Hui-Yan Li, Xi-Le Wei, Bin Deng. 2016. Metabolic Energy of Action Potentials Modulated by Spike Frequency Adaptation. *Frontiers in Neuroscience* **10**. . [[Crossref](#)]
61. D. A. Gray, E. Gabel, T. Blankers, R. M. Hennig. 2016. Multivariate female preference tests reveal latent perceptual biases. *Proceedings of the Royal Society B: Biological Sciences* **283**:1842, 20161972. [[Crossref](#)]
62. Zachary T. McCleney, Zachary P. Kilpatrick. 2016. Entrainment in up and down states of neural populations: non-smooth and stochastic models. *Journal of Mathematical Biology* **73**:5, 1131-1160. [[Crossref](#)]
63. Clarissa J. Whitmire, Garrett B. Stanley. 2016. Rapid Sensory Adaptation Redux: A Circuit Perspective. *Neuron* **92**:2, 298-315. [[Crossref](#)]
64. Yuanyuan Mi, Xiaohan Lin, Si Wu. 2016. Neural Computations in a Dynamical System with Multiple Time Scales. *Frontiers in Computational Neuroscience* **10**. . [[Crossref](#)]
65. Luozheng Li, Wenhao Zhang, Yuanyuan Mi, Dahui Wang, Xiaohan Lin, Si Wu. Dynamical information encoding in neural adaptation 3060-3063. [[Crossref](#)]
66. Laurent Badel, Kazumi Ohta, Yoshiko Tsuchimoto, Hokto Kazama. 2016. Decoding of Context-Dependent Olfactory Behavior in *Drosophila*. *Neuron* **91**:1, 155-167. [[Crossref](#)]
67. Ryota Kobayashi, Katsunori Kitano. 2016. Impact of slow K<sup>+</sup> currents on spike generation can be described by an adaptive threshold model. *Journal of Computational Neuroscience* **40**:3, 347-362. [[Crossref](#)]
68. Bridget N. Ralston, Lucas Q. Flagg, Eric Faggin, John T. Birmingham. 2016. Incorporating spike-rate adaptation into a rate code in mathematical and biological neurons. *Journal of Neurophysiology* **115**:5, 2501-2518. [[Crossref](#)]
69. Erik C. Johnson, Douglas L. Jones, Rama Ratnam. 2016. A minimum-error, energy-constrained neural code is an instantaneous-rate code. *Journal of Computational Neuroscience* **40**:2, 193-206. [[Crossref](#)]
70. H. Francis Song, Guangyu R. Yang, Xiao-Jing Wang. 2016. Training Excitatory-Inhibitory Recurrent Neural Networks for Cognitive Tasks: A Simple and Flexible Framework. *PLoS Computational Biology* **12**:2, e1004792. [[Crossref](#)]
71. Daniel Miner, Jochen Triesch. 2016. Plasticity-Driven Self-Organization under Topological Constraints Accounts for Non-random Features of Cortical Synaptic Wiring. *PLoS Computational Biology* **12**:2, e1004759. [[Crossref](#)]

72. Jason Boulet, Mark White, Ian C. Bruce. 2016. Temporal Considerations for Stimulating Spiral Ganglion Neurons with Cochlear Implants. *Journal of the Association for Research in Otolaryngology* 17:1, 1-17. [[Crossref](#)]
73. Amir Goldental, Pinhas Sabo, Shira Sardi, Roni Vardi, Ido Kanter. 2016. Mimicking Collective Firing Patterns of Hundreds of Connected Neurons using a Single-Neuron Experiment. *Frontiers in Neuroscience* 9. . [[Crossref](#)]
74. Peiji Liang, Si Wu, Fanji Gu. Network Models of Neural Information Processing 293-328. [[Crossref](#)]
75. Sarah Wirtsohn, Bernhard Ronacher. 2016. Response recovery in the locust auditory pathway. *Journal of Neurophysiology* 115:1, 510-519. [[Crossref](#)]
76. Maria Francesca Carfora, Enrica Pirozzi, Luigia Caputo, Aniello Buonocore. 2016. A leaky integrate-and-fire model with adaptation for the generation of a spike train. *Mathematical Biosciences and Engineering* 13:3, 483-493. [[Crossref](#)]
77. Eugenio Urdapilleta. 2015. First-passage-time statistics of a Brownian particle driven by an arbitrary unidimensional potential with a superimposed exponential time-dependent drift. *Journal of Physics A: Mathematical and Theoretical* 48:50, 505001. [[Crossref](#)]
78. Alan Veliz-Cuba, Harel Z. Shouval, Krešimir Josić, Zachary P. Kilpatrick. 2015. Networks that learn the precise timing of event sequences. *Journal of Computational Neuroscience* 39:3, 235-254. [[Crossref](#)]
79. Tilo Schwalger, Benjamin Lindner. 2015. Analytical approach to an integrate-and-fire model with spike-triggered adaptation. *Physical Review E* 92:6. . [[Crossref](#)]
80. David Colliaux, Pierre Yger, Kunihiko Kaneko. 2015. Impact of sub and supra-threshold adaptation currents in networks of spiking neurons. *Journal of Computational Neuroscience* 39:3, 255-270. [[Crossref](#)]
81. Florian Rau, Jan Clemens, Victor Naumov, R. Matthias Hennig, Susanne Schreiber. 2015. Firing-rate resonances in the peripheral auditory system of the cricket, *Gryllus bimaculatus*. *Journal of Comparative Physiology A* 201:11, 1075-1090. [[Crossref](#)]
82. Aniello Buonocore, Luigia Caputo, Giuseppe D'Onofrio, Enrica Pirozzi. 2015. Closed-form solutions for the first-passage-time problem and neuronal modeling. *Ricerche di Matematica* 64:2, 421-439. [[Crossref](#)]
83. Marina Ignatov, Martin Ziegler, Mirko Hansen, Adrian Petraru, Hermann Kohlstedt. 2015. A memristive spiking neuron with firing rate coding. *Frontiers in Neuroscience* 9. . [[Crossref](#)]
84. Lubomir Kostal, Ryota Kobayashi. 2015. Optimal decoding and information transmission in Hodgkin-Huxley neurons under metabolic cost constraints. *Biosystems* 136, 3-10. [[Crossref](#)]
85. Clifford H. Keller, Terry T. Takahashi. 2015. Spike timing precision changes with spike rate adaptation in the owl's auditory space map. *Journal of Neurophysiology* 114:4, 2204-2219. [[Crossref](#)]
86. Jan Clemens, Cyrille C. Girardin, Philip Coen, Xiao-Juan Guan, Barry J. Dickson, Mala Murthy. 2015. Connecting Neural Codes with Behavior in the Auditory System of *Drosophila*. *Neuron* 87:6, 1332-1343. [[Crossref](#)]
87. He Wang, Kin Lam, C. C. Alan Fung, K. Y. Michael Wong, Si Wu. 2015. Rich spectrum of neural field dynamics in the presence of short-term synaptic depression. *Physical Review E* 92:3. . [[Crossref](#)]
88. Arianna Allio, Chiara Calorio, Claudio Franchino, Daniela Gavello, Emilio Carbone, Andrea Marcantoni. 2015. Bud extracts from *Tilia tomentosa* Moench inhibit hippocampal neuronal firing through GABAA and benzodiazepine receptors activation. *Journal of Ethnopharmacology* 172, 288-296. [[Crossref](#)]
89. Alessandra Vitanza, Luca Patané, Paolo Arena. 2015. Spiking neural controllers in multi-agent competitive systems for adaptive targeted motor learning. *Journal of the Franklin Institute* 352:8, 3122-3143. [[Crossref](#)]
90. Tianhe C. Zhang, John J. Janik, Ryan V. Peters, Gang Chen, Ru-Rong Ji, Warren M. Grill. 2015. Spinal sensory projection neuron responses to spinal cord stimulation are mediated by circuits beyond gate control. *Journal of Neurophysiology* 114:1, 284-300. [[Crossref](#)]
91. Douglas L. Jones, Erik C. Johnson, Rama Ratnam. 2015. A stimulus-dependent spike threshold is an optimal neural coder. *Frontiers in Computational Neuroscience* 9. . [[Crossref](#)]
92. Guosheng Yi, Jiang Wang, Kai-Ming Tsang, Xile Wei, Bin Deng, Chunxiao Han. 2015. Spike-frequency adaptation of a two-compartment neuron modulated by extracellular electric fields. *Biological Cybernetics* 109:3, 287-306. [[Crossref](#)]
93. LieJune Shiau, Tilo Schwalger, Benjamin Lindner. 2015. Interspike interval correlation in a stochastic exponential integrate-and-fire model with subthreshold and spike-triggered adaptation. *Journal of Computational Neuroscience* 38:3, 589-600. [[Crossref](#)]
94. Guosheng Yi, Jiang Wang, Bin Deng, Xile Wei. 2015. Spike initiating dynamics of the neuron with different adaptation mechanisms to extracellular electric fields. *Communications in Nonlinear Science and Numerical Simulation* 22:1-3, 574-586. [[Crossref](#)]
95. Eugenio Urdapilleta, Inés Samengo. 2015. Effects of spike-triggered negative feedback on receptive-field properties. *Journal of Computational Neuroscience* 38:2, 405-425. [[Crossref](#)]

96. K. Jannis Hildebrandt, Bernhard Ronacher, R. Matthias Hennig, Jan Benda. 2015. A Neural Mechanism for Time-Window Separation Resolves Ambiguity of Adaptive Coding. *PLoS Biology* **13**:3, e1002096. [[Crossref](#)]
97. C. C. Alan Fung, S.-i. Amari. 2015. Spontaneous Motion on Two-Dimensional Continuous Attractors. *Neural Computation* **27**:3, 507-547. [[Abstract](#)] [[Full Text](#)] [[PDF](#)] [[PDF Plus](#)]
98. Vahab Yousofzadeh, Girijesh Prasad, KongFatt Wong-Lin. 2015. On self-feedback connectivity in neural mass models applied to event-related potentials. *NeuroImage* **108**, 364-376. [[Crossref](#)]
99. Hinrich Arnoldt, Shuwen Chang, Sven Jahnke, Birk Urmersbach, Holger Taschenberger, Marc Timme. 2015. When Less Is More: Non-monotonic Spike Sequence Processing in Neurons. *PLoS Computational Biology* **11**:2, e1004002. [[Crossref](#)]
100. Brian Nils Lundstrom. 2015. Modeling multiple time scale firing rate adaptation in a neural network of local field potentials. *Journal of Computational Neuroscience* **38**:1, 189-202. [[Crossref](#)]
101. K. Jannis Hildebrandt, Jan Benda, R. Matthias Hennig. 2015. Computational themes of peripheral processing in the auditory pathway of insects. *Journal of Comparative Physiology A* **201**:1, 39-50. [[Crossref](#)]
102. Carlo R. Laing. 2015. Exact Neural Fields Incorporating Gap Junctions. *SIAM Journal on Applied Dynamical Systems* **14**:4, 1899-1929. [[Crossref](#)]
103. G. Deco, P. Hagmann, A. G. Hudetz, G. Tononi. 2014. Modeling Resting-State Functional Networks When the Cortex Falls Asleep: Local and Global Changes. *Cerebral Cortex* **24**:12, 3180-3194. [[Crossref](#)]
104. Moritz Deger, Tilo Schwalger, Richard Naud, Wulfram Gerstner. 2014. Fluctuations and information filtering in coupled populations of spiking neurons with adaptation. *Physical Review E* **90**:6. . [[Crossref](#)]
105. Hil GE Meijer, Stephen Coombes. 2014. Travelling waves in models of neural tissue: from localised structures to periodic waves. *EPJ Nonlinear Biomedical Physics* **2**:1. . [[Crossref](#)]
106. Christian RÄssert, Sergio Solinas, Egidio D'Angelo, Paul Dean, John Porrill. 2014. Model cerebellar granule cells can faithfully transmit modulated firing rate signals. *Frontiers in Cellular Neuroscience* **8**. . [[Crossref](#)]
107. Justus A. Kromer, Reynaldo D. Pinto, Benjamin Lindner, Lutz Schimansky-Geier. 2014. Noise-controlled bistability in an excitable system with positive feedback. *EPL (Europhysics Letters)* **108**:2, 20007. [[Crossref](#)]
108. Loreen HertÄg, Daniel Durstewitz, Nicolas Brunel. 2014. Analytical approximations of the firing rate of an adaptive exponential integrate-and-fire neuron in the presence of synaptic noise. *Frontiers in Computational Neuroscience* **8**. . [[Crossref](#)]
109. Henriette Walz, Jan Grewe, Jan Benda. 2014. Static frequency tuning accounts for changes in neural synchrony evoked by transient communication signals. *Journal of Neurophysiology* **112**:4, 752-765. [[Crossref](#)]
110. Shiyun Meng. 2014. Nerve cell differentiation using constant and programmed electrical stimulation through conductive non-functional graphene nanosheets film. *Tissue Engineering and Regenerative Medicine* **11**:4, 274-283. [[Crossref](#)]
111. Gabriel Koch Ocker, Brent Doiron. 2014. Kv7 channels regulate pairwise spiking covariability in health and disease. *Journal of Neurophysiology* **112**:2, 340-352. [[Crossref](#)]
112. Andrea Marcantoni, Elisabeth F. Raymond, Emilio Carbone, HÄlÄne Marie. 2014. Firing properties of entorhinal cortex neurons and early alterations in an Alzheimer's disease transgenic model. *Pflügers Archiv - European Journal of Physiology* **466**:7, 1437-1450. [[Crossref](#)]
113. Henry C. Tuckwell, Nicholas J. Penington. 2014. Computational modeling of spike generation in serotonergic neurons of the dorsal raphe nucleus. *Progress in Neurobiology* **118**, 59-101. [[Crossref](#)]
114. Carlo R. Laing. 2014. Derivation of a neural field model from a network of theta neurons. *Physical Review E* **90**:1. . [[Crossref](#)]
115. Ardalan Aarabi, Bin He. 2014. Seizure prediction in hippocampal and neocortical epilepsy using a model-based approach. *Clinical Neurophysiology* **125**:5, 930-940. [[Crossref](#)]
116. Yunyan Wang, Yoram Gutfreund, JosÄ© L. PeÄ±a. 2014. Coding space-time stimulus dynamics in auditory brain maps. *Frontiers in Physiology* **5**. . [[Crossref](#)]
117. Wondimu Teka, Toma M. Marinov, Fidel Santamaria. 2014. Neuronal Spike Timing Adaptation Described with a Fractional Leaky Integrate-and-Fire Model. *PLoS Computational Biology* **10**:3, e1003526. [[Crossref](#)]
118. Navid Khosravi-Hashemi, Maurice J. Chacron. 2014. Motion processing across multiple topographic maps in the electrosensory system. *Physiological Reports* **2**:3, e00253. [[Crossref](#)]
119. Justus A. Kromer, Benjamin Lindner, Lutz Schimansky-Geier. 2014. Event-triggered feedback in noise-driven phase oscillators. *Physical Review E* **89**:3. . [[Crossref](#)]
120. Josef Ladenbauer, Moritz Augustin, Klaus Obermayer. 2014. How adaptation currents change threshold, gain, and variability of neuronal spiking. *Journal of Neurophysiology* **111**:5, 939-953. [[Crossref](#)]

121. Jan Benda, Joel Tabak. Spike-Frequency Adaptation 1-12. [[Crossref](#)]
122. Klaus Wimmer. Adaptation in Sensory Cortices, Models of 1-6. [[Crossref](#)]
123. Paul C. Bressloff. Single Neuron Modeling 3-62. [[Crossref](#)]
124. Paul C. Bressloff. Traveling Waves in One-Dimensional Excitable Media 63-99. [[Crossref](#)]
125. Paul C. Bressloff. Wave Propagation Along Spiny Dendrites 101-136. [[Crossref](#)]
126. Paul C. Bressloff. Calcium Waves and Sparks 137-181. [[Crossref](#)]
127. Paul C. Bressloff. Waves in Synaptically Coupled Spiking Networks 185-231. [[Crossref](#)]
128. Paul C. Bressloff. Population Models and Neural Fields 233-269. [[Crossref](#)]
129. Paul C. Bressloff. Waves in Excitable Neural Fields 271-318. [[Crossref](#)]
130. Paul C. Bressloff. Neural Field Model of Binocular Rivalry Waves 319-345. [[Crossref](#)]
131. Paul C. Bressloff. Waves in the Developing and the Diseased Brain 349-404. [[Crossref](#)]
132. Benjamin Lindner. Low-Pass Filtering of Information in the Leaky Integrate-and-Fire Neuron Driven by White Noise 249-258. [[Crossref](#)]
133. Andreas Stumpner, Manuela Nowotny. Neural Processing in the Bush-Cricket Auditory Pathway 143-166. [[Crossref](#)]
134. G. Bard Ermentrout, Stefanos E. Folias, Zachary P. Kilpatrick. Spatiotemporal Pattern Formation in Neural Fields with Linear Adaptation 119-151. [[Crossref](#)]
135. Zachary P. Kilpatrick, Grégory Faye. 2014. Pulse Bifurcations in Stochastic Neural Fields. *SIAM Journal on Applied Dynamical Systems* 13:2, 830-860. [[Crossref](#)]
136. Friedemann Zenke, Guillaume Hennequin, Wulfram Gerstner. 2013. Synaptic Plasticity in Neural Networks Needs Homeostasis with a Fast Rate Detector. *PLoS Computational Biology* 9:11, e1003330. [[Crossref](#)]
137. Chris Häusler, Alex Susemihl, Martin P. Nawrot. 2013. Natural image sequences constrain dynamic receptive fields and imply a sparse code. *Brain Research* 1536, 53-67. [[Crossref](#)]
138. N. G. Bibikov. 2013. On the existence of spontaneous neuronal bursting activity at the periphery of the amphibian auditory pathway. *Journal of Evolutionary Biochemistry and Physiology* 49:6, 579-591. [[Crossref](#)]
139. Farzad Farkhooi, Anja Froese, Eilif Muller, Randolph Menzel, Martin P. Nawrot. 2013. Cellular Adaptation Facilitates Sparse and Reliable Coding in Sensory Pathways. *PLoS Computational Biology* 9:10, e1003251. [[Crossref](#)]
140. T. Schwalger, D. Miklody, B. Lindner. 2013. When the leak is weak – how the first-passage statistics of a biased random walk can approximate the ISI statistics of an adapting neuron. *The European Physical Journal Special Topics* 222:10, 2655-2666. [[Crossref](#)]
141. S. E. Clarke, R. Naud, A. Longtin, L. Maler. 2013. Speed-invariant encoding of looming object distance requires power law spike rate adaptation. *Proceedings of the National Academy of Sciences* 110:33, 13624-13629. [[Crossref](#)]
142. Christian Pozzorini, Richard Naud, Skander Mensi, Wulfram Gerstner. 2013. Temporal whitening by power-law adaptation in neocortical neurons. *Nature Neuroscience* 16:7, 942-948. [[Crossref](#)]
143. Jiang Wang, Kuan Wang, Li Chang, Bin Deng, Xile Wei, Huiyan Li. The effect of direct-current field on the adaptability in the minimal model 2662-2666. [[Crossref](#)]
144. Nahal Sharafi, Jan Benda, Benjamin Lindner. 2013. Information filtering by synchronous spikes in a neural population. *Journal of Computational Neuroscience* 34:2, 285-301. [[Crossref](#)]
145. Chang-Hee Kim, Jae Jin Shin, Jun Kim, Sang Jeong Kim. 2013. Reduced spike frequency adaptation in Purkinje cells of the vestibulocerebellum. *Neuroscience Letters* 535, 45-50. [[Crossref](#)]
146. R. Matthias Hennig, Bernhard Ronacher. Auditory Processing in Insects 1-23. [[Crossref](#)]
147. J.M. Ball, A.M. Hummos, S.S. Nair. 2012. Role of sensory input distribution and intrinsic connectivity in lateral amygdala during auditory fear conditioning: A computational study. *Neuroscience* 224, 249-267. [[Crossref](#)]
148. Tara Deemyad, Jens Kroeger, Maurice J. Chacron. 2012. Sub- and suprathreshold adaptation currents have opposite effects on frequency tuning. *The Journal of Physiology* 590:19, 4839-4858. [[Crossref](#)]
149. Jesus M. Cortes, Daniele Marinazzo, Peggy Series, Mike W. Oram, Terry J. Sejnowski, Mark C. W. van Rossum. 2012. The effect of neural adaptation on population coding accuracy. *Journal of Computational Neuroscience* 32:3, 387-402. [[Crossref](#)]
150. Suren Jayasuriya, Zachary P. Kilpatrick. 2012. Effects of Time-Dependent Stimuli in a Competitive Neural Network Model of Perceptual Rivalry. *Bulletin of Mathematical Biology* 74:6, 1396-1426. [[Crossref](#)]
151. Eugenio Urdapilleta. 2012. Series solution to the first-passage-time problem of a Brownian motion with an exponential time-dependent drift. *Journal of Physics A: Mathematical and Theoretical* 45:18, 185001. [[Crossref](#)]

152. Martin Paul Nawrot. 2012. Dynamics of sensory processing in the dual olfactory pathway of the honeybee. *Apidologie* 43:3, 269-291. [[Crossref](#)]
153. Jiang Wang, Li Chang, Bin Deng, Xile Wei, Huiyan Li. The effect of extreme low frequency external alternating-current field on the adaptability in the Ermentrout model 123-128. [[Crossref](#)]
154. Li Chang, Jiang Wang, Bin Deng, Xile Wei, Huiyan Li. 2012. The effect of extreme low frequency external electric field on the adaptability in the Ermentrout model. *Neurocomputing* 81, 67-74. [[Crossref](#)]
155. Skander Mensi, Richard Naud, Christian Pozzorini, Michael Avermann, Carl C. H. Petersen, Wulfram Gerstner. 2012. Parameter extraction and classification of three cortical neuron types reveals two distinct adaptation mechanisms. *Journal of Neurophysiology* 107:6, 1756-1775. [[Crossref](#)]
156. Zachary P. Kilpatrick, G. Bard Ermentrout. 2012. Hallucinogen persisting perception disorder in neuronal networks with adaptation. *Journal of Computational Neuroscience* 32:1, 25-53. [[Crossref](#)]
157. Martin Singheiser, Roland Ferger, Mark von Campenhausen, Hermann Wagner. 2012. Adaptation in the auditory midbrain of the barn owl (*Tyto alba*) induced by tonal double stimulation. *European Journal of Neuroscience* 35:3, 445-456. [[Crossref](#)]
158. Paul C Bressloff. 2012. Spatiotemporal dynamics of continuum neural fields. *Journal of Physics A: Mathematical and Theoretical* 45:3, 033001. [[Crossref](#)]
159. Rafael Kurtz. Adaptive encoding of motion information in the fly visual system 115-128. [[Crossref](#)]
160. Richard Naud, Wulfram Gerstner. The Performance (and Limits) of Simple Neuron Models: Generalizations of the Leaky Integrate-and-Fire Model 163-192. [[Crossref](#)]
161. Eugenio Urdapilleta. 2011. Onset of negative interspike interval correlations in adapting neurons. *Physical Review E* 84:4. . [[Crossref](#)]
162. Jeremie Lefebvre, Andre Longtin, Victor G. LeBlanc. 2011. Neural adaptation facilitates oscillatory responses to static inputs in a recurrent network of ON and OFF cells. *Journal of Computational Neuroscience* 31:1, 73-86. [[Crossref](#)]
163. Adam D. Schneider, Kathleen E. Cullen, Maurice J. Chacron. 2011. In vivo Conditions Induce Faithful Encoding of Stimuli by Reducing Nonlinear Synchronization in Vestibular Sensory Neurons. *PLoS Computational Biology* 7:7, e1002120. [[Crossref](#)]
164. Azadeh Khajeh Alijani, Magnus J. E. Richardson. 2011. Rate response of neurons subject to fast or frozen noise: From stochastic and homogeneous to deterministic and heterogeneous populations. *Physical Review E* 84:1. . [[Crossref](#)]
165. Gustavo Deco, Alexander Thiele. 2011. Cholinergic control of cortical network interactions enables feedback-mediated attentional modulation. *European Journal of Neuroscience* 34:1, 146-157. [[Crossref](#)]
166. B. Cessac. 2011. A discrete time neural network model with spiking neurons: II: Dynamics with noise. *Journal of Mathematical Biology* 62:6, 863-900. [[Crossref](#)]
167. Oscar Avila-Akerberg, Maurice J. Chacron. 2011. Nonrenewal spike train statistics: causes and functional consequences on neural coding. *Experimental Brain Research* 210:3-4, 353-371. [[Crossref](#)]
168. C. Rössert, H. Straka. 2011. Interactions between intrinsic membrane and emerging network properties determine signal processing in central vestibular neurons. *Experimental Brain Research* 210:3-4, 437-449. [[Crossref](#)]
169. Collins Assisi, Mark Stopfer, Maxim Bazhenov. 2011. Using the Structure of Inhibitory Networks to Unravel Mechanisms of Spatiotemporal Patterning. *Neuron* 69:2, 373-386. [[Crossref](#)]
170. J.F.M. van Brederode, A. J. Berger. 2011. GAD67-GFP+ Neurons in the Nucleus of Roller. II. Subthreshold and Firing Resonance Properties. *Journal of Neurophysiology* 105:1, 249-278. [[Crossref](#)]
171. Tilo Schwalger, Karin Fisch, Jan Benda, Benjamin Lindner. 2010. How Noisy Adaptation of Neurons Shapes Interspike Interval Histograms and Correlations. *PLoS Computational Biology* 6:12, e1001026. [[Crossref](#)]
172. Jan Benda, Leonard Maler, André Longtin. 2010. Linear Versus Nonlinear Signal Transmission in Neuron Models With Adaptation Currents or Dynamic Thresholds. *Journal of Neurophysiology* 104:5, 2806-2820. [[Crossref](#)]
173. Yann Le Franc, Gwendal Le Masson. 2010. Multiple Firing Patterns in Deep Dorsal Horn Neurons of the Spinal Cord: Computational Analysis of Mechanisms and Functional Implications. *Journal of Neurophysiology* 104:4, 1978-1996. [[Crossref](#)]
174. Abhilash Ponnath, Hamilton E. Farris. 2010. Calcium-dependent control of temporal processing in an auditory interneuron: a computational analysis. *Journal of Comparative Physiology A* 196:9, 613-628. [[Crossref](#)]
175. T. Schwalger, B. Lindner. 2010. Theory for serial correlations of interevent intervals. *The European Physical Journal Special Topics* 187:1, 211-221. [[Crossref](#)]
176. Kurtis D. Cantley, Anand Subramaniam, Harvey J. Stiegler, Richard A. Chapman, Eric M. Vogel. SPICE simulation of nanoscale non-crystalline silicon TFTs in spiking neuron circuits 1202-1205. [[Crossref](#)]

177. Felix Creutzig, Jan Benda, Sandra Wohlge-muth, Andreas Stumpner, Bernhard Ronacher, Andreas V. M. Herz. 2010. Timescale-Invariant Pattern Recognition by Feedforward Inhibition and Parallel Signal Processing. *Neural Computation* **22**:6, 1493-1510. [[Abstract](#)] [[Full Text](#)] [[PDF](#)] [[PDF Plus](#)]
178. Zachary P. Kilpatrick, Paul C. Bressloff. 2010. Stability of bumps in piecewise smooth neural fields with nonlinear adaptation. *Physica D: Nonlinear Phenomena* **239**:12, 1048-1060. [[Crossref](#)]
179. Zachary P. Kilpatrick, Paul C. Bressloff. 2010. Effects of synaptic depression and adaptation on spatiotemporal dynamics of an excitatory neuronal network. *Physica D: Nonlinear Phenomena* **239**:9, 547-560. [[Crossref](#)]
180. Jan Clemens, Gerroth Weschke, Astrid Vogel, Bernhard Ronacher. 2010. Intensity invariance properties of auditory neurons compared to the statistics of relevant natural signals in grasshoppers. *Journal of Comparative Physiology A* **196**:4, 285-297. [[Crossref](#)]
181. Zachary P. Kilpatrick, Paul C. Bressloff. 2010. Spatially structured oscillations in a two-dimensional excitatory neuronal network with synaptic depression. *Journal of Computational Neuroscience* **28**:2, 193-209. [[Crossref](#)]
182. P. D'Souza, S.-C. Liu, R. H. R. Hahnloser. 2010. Perceptron learning rule derived from spike-frequency adaptation and spike-time-dependent plasticity. *Proceedings of the National Academy of Sciences* **107**:10, 4722-4727. [[Crossref](#)]
183. Bryan P. Tripp, Chris Eliasmith. 2010. Population Models of Temporal Differentiation. *Neural Computation* **22**:3, 621-659. [[Abstract](#)] [[Full Text](#)] [[PDF](#)] [[PDF Plus](#)]
184. Martin Paul Nawrot. Analysis and Interpretation of Interval and Count Variability in Neural Spike Trains 37-58. [[Crossref](#)]
185. Eugenio Urdapilleta, Inés Samengo. 2009. The firing statistics of Poisson neuron models driven by slow stimuli. *Biological Cybernetics* **101**:4, 265-277. [[Crossref](#)]
186. Natalia Toporikova, Maurice J. Chacron. 2009. SK Channels Gate Information Processing In Vivo by Regulating an Intrinsic Bursting Mechanism Seen In Vitro. *Journal of Neurophysiology* **102**:4, 2273-2287. [[Crossref](#)]
187. Zachary P Kilpatrick, Paul C Bressloff. 2009. Oscillations in an excitatory neuronal network with synaptic depression and adaptation. *BMC Neuroscience* **10**:S1. . [[Crossref](#)]
188. Magnus J. E. Richardson. 2009. Dynamics of populations and networks of neurons with voltage-activated and calcium-activated currents. *Physical Review E* **80**:2. . [[Crossref](#)]
189. Eugenio Urdapilleta, Inés Samengo. 2009. Quasistatic approximation of the interspike interval distribution of neurons driven by time-dependent inputs. *Physical Review E* **80**:1. . [[Crossref](#)]
190. Jianxia Cui, Carmen C. Canavier, Robert J. Butera. 2009. Functional Phase Response Curves: A Method for Understanding Synchronization of Adapting Neurons. *Journal of Neurophysiology* **102**:1, 387-398. [[Crossref](#)]
191. Simon Peter Peron, Fabrizio Gabbiani. 2009. Role of spike-frequency adaptation in shaping neuronal response to dynamic stimuli. *Biological Cybernetics* **100**:6, 505-520. [[Crossref](#)]
192. E. Alvarez-Lacalle, E. Moses. 2009. Slow and fast pulses in 1-D cultures of excitatory neurons. *Journal of Computational Neuroscience* **26**:3, 475-493. [[Crossref](#)]
193. Farzad Farkhooi, Martin F. Strube-Bloss, Martin P. Nawrot. 2009. Serial correlation in neural spike trains: Experimental evidence, stochastic modeling, and single neuron variability. *Physical Review E* **79**:2. . [[Crossref](#)]
194. Ryota Kobayashi. 2009. The influence of firing mechanisms on gain modulation. *Journal of Statistical Mechanics: Theory and Experiment* **2009**:01, P01017. [[Crossref](#)]
195. Richard Naud, Nicolas Marcille, Claudia Clopath, Wulfram Gerstner. 2008. Firing patterns in the adaptive exponential integrate-and-fire model. *Biological Cybernetics* **99**:4-5, 335-347. [[Crossref](#)]
196. Michele Giugliano, Giancarlo La Camera, Stefano Fusi, Walter Senn. 2008. The response of cortical neurons to in vivo-like input current: theory and experiment: II. Time-varying and spatially distributed inputs. *Biological Cybernetics* **99**:4-5, 303-318. [[Crossref](#)]
197. Giancarlo La Camera, Michele Giugliano, Walter Senn, Stefano Fusi. 2008. The response of cortical neurons to in vivo-like input current: theory and experiment. *Biological Cybernetics* **99**:4-5, 279-301. [[Crossref](#)]
198. Brian N Lundstrom, Matthew H Higgs, William J Spain, Adrienne L Fairhall. 2008. Fractional differentiation by neocortical pyramidal neurons. *Nature Neuroscience* **11**:11, 1335-1342. [[Crossref](#)]
199. Klaus Wimmer, K. Jannis Hildebrandt, R. Matthias Hennig, Klaus Obermayer. 2008. Adaptation and Selective Information Transmission in the Cricket Auditory Neuron AN2. *PLoS Computational Biology* **4**:9, e1000182. [[Crossref](#)]
200. T. A. Engel, L. Schimansky-Geier, A.V.M. Herz, S. Schreiber, I. Erchova. 2008. Subthreshold Membrane-Potential Resonances Shape Spike-Train Patterns in the Entorhinal Cortex. *Journal of Neurophysiology* **100**:3, 1576-1589. [[Crossref](#)]

201. R.J. Moran, K.E. Stephan, S.J. Kiebel, N. Rombach, W.T. O'Connor, K.J. Murphy, R.B. Reilly, K.J. Friston. 2008. Bayesian estimation of synaptic physiology from the spectral responses of neural masses. *NeuroImage* **42**:1, 272-284. [[Crossref](#)]
202. Rüdiger Krahe, Joseph Bastian, Maurice J. Chacron. 2008. Temporal Processing Across Multiple Topographic Maps in the Electrosensory System. *Journal of Neurophysiology* **100**:2, 852-867. [[Crossref](#)]
203. Sungho Hong, Brian Nils Lundstrom, Adrienne L. Fairhall. 2008. Intrinsic Gain Modulation and Adaptive Neural Coding. *PLoS Computational Biology* **4**:7, e1000119. [[Crossref](#)]
204. Brian Nils Lundstrom, Sungho Hong, Matthew H. Higgs, Adrienne L. Fairhall. 2008. Two Computational Regimes of a Single-Compartment Neuron Separated by a Planar Boundary in Conductance Space. *Neural Computation* **20**:5, 1239-1260. [[Abstract](#)] [[PDF](#)] [[PDF Plus](#)]
205. W. Hamish Mehaffey, Leonard Maler, Ray W. Turner. 2008. Intrinsic Frequency Tuning in ELL Pyramidal Cells Varies Across Electrosensory Maps. *Journal of Neurophysiology* **99**:5, 2641-2655. [[Crossref](#)]
206. Jan Benda, R. Matthias Hennig. 2008. Spike-frequency adaptation generates intensity invariance in a primary auditory interneuron. *Journal of Computational Neuroscience* **24**:2, 113-136. [[Crossref](#)]
207. Renaud Jolivet, Ryota Kobayashi, Alexander Rauch, Richard Naud, Shigeru Shinomoto, Wulfram Gerstner. 2008. A benchmark test for a quantitative assessment of simple neuron models. *Journal of Neuroscience Methods* **169**:2, 417-424. [[Crossref](#)]
208. Gerroth Weschke, Bernhard Ronacher. 2008. Influence of sound pressure level on the processing of amplitude modulations by auditory neurons of the locust. *Journal of Comparative Physiology A* **194**:3, 255-265. [[Crossref](#)]
209. Irina Erchova, David J. McGonigle. 2008. Rhythms of the brain: An examination of mixed mode oscillation approaches to the analysis of neurophysiological data. *Chaos: An Interdisciplinary Journal of Nonlinear Science* **18**:1, 015115. [[Crossref](#)]
210. B. Hedwig, G.S. Pollack. Invertebrate Auditory Pathways 525-564. [[Crossref](#)]
211. Tim Gollisch. 2008. Time-warp invariant pattern detection with bursting neurons. *New Journal of Physics* **10**:1, 015012. [[Crossref](#)]
212. Eilif Muller, Lars Buesing, Johannes Schemmel, Karlheinz Meier. 2007. Spike-Frequency Adapting Neural Ensembles: Beyond Mean Adaptation and Renewal Theories. *Neural Computation* **19**:11, 2958-3010. [[Abstract](#)] [[PDF](#)] [[PDF Plus](#)]
213. Jacobo D. Sitt, J. Aliaga. 2007. Versatile biologically inspired electronic neuron. *Physical Review E* **76**:5. . [[Crossref](#)]
214. Kirill Ukhanov, Trese Leinders-Zufall, Frank Zufall. 2007. Patch-Clamp Analysis of Gene-Targeted Vomeronasal Neurons Expressing a Defined V1r or V2r Receptor: Ionic Mechanisms Underlying Persistent Firing. *Journal of Neurophysiology* **98**:4, 2357-2369. [[Crossref](#)]
215. R.J. Moran, S.J. Kiebel, K.E. Stephan, R.B. Reilly, J. Daunizeau, K.J. Friston. 2007. A neural mass model of spectral responses in electrophysiology. *NeuroImage* **37**:3, 706-720. [[Crossref](#)]
216. Barry Wark, Brian Nils Lundstrom, Adrienne Fairhall. 2007. Sensory adaptation. *Current Opinion in Neurobiology* **17**:4, 423-429. [[Crossref](#)]
217. P. N. Loxley, P. A. Robinson. 2007. Spike-rate adaptation and neuronal bursting in a mean-field model of brain activity. *Biological Cybernetics* **97**:2, 113-122. [[Crossref](#)]
218. Guido Gigante, Paolo Del Giudice, Maurizio Mattia. 2007. Frequency-dependent response properties of adapting spiking neurons. *Mathematical Biosciences* **207**:2, 336-351. [[Crossref](#)]
219. Martin P. Nawrot, Clemens Boucsein, Victor Rodriguez-Molina, Ad Aertsen, Sonja Grün, Stefan Rotter. 2007. Serial interval statistics of spontaneous activity in cortical neurons in vivo and in vitro. *Neurocomputing* **70**:10-12, 1717-1722. [[Crossref](#)]
220. Guido Gigante, Maurizio Mattia, Paolo Del Giudice. 2007. Diverse Population-Bursting Modes of Adapting Spiking Neurons. *Physical Review Letters* **98**:14. . [[Crossref](#)]
221. Daniel Gussin, Jan Benda, Leonard Maler. 2007. Limits of Linear Rate Coding of Dynamic Stimuli by Electroreceptor Afferents. *Journal of Neurophysiology* **97**:4, 2917-2929. [[Crossref](#)]
222. Raul C. Muresan, Cristina Savin. 2007. Resonance or Integration? Self-Sustained Dynamics and Excitability of Neural Microcircuits. *Journal of Neurophysiology* **97**:3, 1911-1930. [[Crossref](#)]
223. Ulrich Beckers, Martin Egelhaaf, Rafael Kurtz. 2007. Synapses in the Fly Motion-Vision Pathway: Evidence for a Broad Range of Signal Amplitudes and Dynamics. *Journal of Neurophysiology* **97**:3, 2032-2041. [[Crossref](#)]
224. Michael A. Nordstrom, Robert B. Gorman, Yiannis Laouris, John M. Spielmann, Douglas G. Stuart. 2007. Does motoneuron adaptation contribute to muscle fatigue?. *Muscle & Nerve* **35**:2, 135-158. [[Crossref](#)]
225. Marylka Uusisaari, Kunihiko Obata, Thomas Knöpfel. 2007. Morphological and Electrophysiological Properties of GABAergic and Non-GABAergic Cells in the Deep Cerebellar Nuclei. *Journal of Neurophysiology* **97**:1, 901-911. [[Crossref](#)]

226. Fabrizio Gabbiani, Holger G. Krapp. 2006. Spike-Frequency Adaptation and Intrinsic Properties of an Identified, Looming-Sensitive Neuron. *Journal of Neurophysiology* **96**:6, 2951-2962. [[Crossref](#)]
227. Martin Greschner, Andreas Thiel, Jutta Kretzberg, Josef Ammermüller. 2006. Complex Spike-Event Pattern of Transient on-off Retinal Ganglion Cells. *Journal of Neurophysiology* **96**:6, 2845-2856. [[Crossref](#)]
228. Jan Benda, André Longtin, Leonard Maler. 2006. A Synchronization-Desynchronization Code for Natural Communication Signals. *Neuron* **52**:2, 347-358. [[Crossref](#)]
229. Renaud Jolivet, Alexander Rauch, Hans-Rudolf Lüscher, Wulfram Gerstner. 2006. Predicting spike timing of neocortical pyramidal neurons by simple threshold models. *Journal of Computational Neuroscience* **21**:1, 35-49. [[Crossref](#)]
230. A. N. Burkitt. 2006. A Review of the Integrate-and-fire Neuron Model: I. Homogeneous Synaptic Input. *Biological Cybernetics* **95**:1, 1-19. [[Crossref](#)]
231. Yanan Zheng, James McDougal, Rory Conolly, Qiang Zhang. Biologically Based Pharmacokinetic and Pharmacodynamic Models of the Skin 89-112. [[Crossref](#)]
232. B. Naundorf, T. Geisel, F. Wolf. 2005. Action Potential Onset Dynamics and the Response Speed of Neuronal Populations. *Journal of Computational Neuroscience* **18**:3, 297-309. [[Crossref](#)]
233. Roland Schaette, Tim Gollisch, Andreas V. M. Herz. 2005. Spike-Train Variability of Auditory Neurons In Vivo: Dynamic Responses Follow Predictions From Constant Stimuli. *Journal of Neurophysiology* **93**:6, 3270-3281. [[Crossref](#)]
234. Raymon M. Glantz, John P. Schroeter. 2004. Analysis and Simulation of Gain Control and Precision in Crayfish Visual Interneurons. *Journal of Neurophysiology* **92**:5, 2747-2761. [[Crossref](#)]
235. Renaud Jolivet, Timothy J. Lewis, Wulfram Gerstner. 2004. Generalized Integrate-and-Fire Models of Neuronal Activity Approximate Spike Trains of a Detailed Model to a High Degree of Accuracy. *Journal of Neurophysiology* **92**:2, 959-976. [[Crossref](#)]
236. Raymon M. Glantz, John P. Schroeter. 2004. Encoder Adaptation Modulates the Visual Responses of Crayfish Interneurons. *Journal of Neurophysiology* **92**:1, 327-340. [[Crossref](#)]